

Altered development in rodent brain cells after 900 MHz radiofrequency exposure

Raphaël Bodin^{a,*,1}, Lucas Godin^{a,1}, Camille Mougin^{a,c}, Anthony Lecomte^a,
Vanessa Larrigaldie^c, Justyne Feat-Vetel^c, Sarah Méresse^c, Céline Montécot-Dubourg^{c,d},
Paulo Marcelo^b, Stéphane Mortaud^{c,d}, Anne-Sophie Villegier^a

^a PERITOX Laboratory (UMR_I 01), UPJV/INERIS INERIS, MIV/TEAM, Verneuil-en-Halatte France University of Picardie Jules Verne, CURS, Amiens, France

^b Plateforme ICAP, Centre Universitaire de Recherche en Santé, University of Picardie Jules Verne, CURS, Amiens, France

^c Immuno-Neuro Modulation - UMR7355, 3B rue de la Férollerie, Orleans Cedex 2 F-45071, France

^d Orleans University, Orleans, France

ARTICLE INFO

Keywords:

Radiofrequency fields
Proliferation
Synaptogenesis
Neuroproteomics
Neurodevelopment
Neurotoxicology
Stem cells

ABSTRACT

Health risks related to 900 MHz 2 G frequency exposure remain inconclusive under current regulatory standards. Research into potential long-term effects is ongoing, particularly as the use of mobile networks and wireless devices increases. This study investigates the effects of non-thermal exposure levels of mobile phone 900 MHz radiofrequency electromagnetic field (RF-EMF) on rodent neurodevelopment. *In vivo*, the effects of pre- and post-natal 0.08 and 0.4 W/kg specific absorption rate (SAR) exposure were assessed for their impact on the proteomic profile at postnatal day 0 (PND 0). Brain-derived neurotrophic factor (BDNF), BrdU+ proliferative cells, synaptogenesis, and oxidative stress in the hippocampus and cortex of rat pups were studied at PND 8 and PND 17. Effects of the lowest SAR (0.08 W/kg) were assessed *in vitro* to afford mechanistic data regarding neural stem cells (NSCs) differentiation. *In vivo* results showed a decrease in BDNF level and BrdU+ proliferative cells with a decrease in synapse balance (excitatory synapses/inhibitory synapses). *In vitro*, at 0.08 W/kg there was an increase in Ki-67 + proliferative cells, apoptosis, and double-strand DNA breaks in NSCs. A lower ratio of B1 cells (primary progenitors of NSCs) among total cerebral cells and a higher ratio of oligodendrocyte progenitor cells and astrocytes were observed in the exposed NSCs. Our findings suggest that key cellular events for brain ontogenesis are likely to undergo changes with RF-EMF 900 MHz exposure during early development. These support the hypothesis that the developing central nervous system is vulnerable to RF-EMF exposures in rodents at regulatory thresholds.

1. Introduction

Radiofrequency electromagnetic field (RF-EMF) exposure is present in the environment in both urban and rural areas. To protect populations and to limit exposures, thresholds of 51.96 V/m for occupational environments and 35.17 V/m for general public environments were set by the International Commission on Non-Ionizing Radiation Protection (ICNIRP) for 900 MHz. The specific absorption rate (SAR) defines the tissue-absorbed energy per unit of mass. The ICNIRP recommends a SAR of 0.08 W/kg for the public and 0.4 W/kg for occupational limits. Occupational environments may involve higher levels (Vali^ć et al., 2012, 2017; Gallucci et al., 2022), but mean levels in public

environments are about 15–60 times lower than these limits. For example measurements in Australia indicated 4.33 V/m in the city centers and 0.75 V/m in outdoor and residential areas or parks (Bhatt et al., 2016). Yet, studies on non-thermal RF-EMF exposure during the gestational and early postnatal period (until weaning) suggested oxidative damage in the brain (Sharma et al., 2021). In our previous study we reported accelerated physical developments and reduced body weight in pre- and post-natal exposed rat pups at 900 MHz (Bodin et al., 2024). In the context of the Developmental Origins of Health and Disease (DOHaD) hypothesis, early-life exposure to neurotoxicants may have enduring implications for neurodevelopmental trajectories (Grandjean and Landrigan, 2014; Albores-Garcia et al., 2021).

* Correspondence to: Rue Jacques Taffanel, Verneuil-en-Halatte 60550, France.

E-mail address: Bodin.raphael85@gmail.com (R. Bodin).

¹ Co-first authorship

Around gestational day (GD) 10–12 in mice, the neuroepithelial stem cells (NSC) evolve into radial glial progenitor cells (RGPs). In the embryonic brain of vertebrates, RGPs will proliferate, giving rise to progenitor cells and can undergo asymmetric differentiation into neuronal and glial cells (Haubensak et al., 2004; Noctor et al., 2004; Rowitch and Kriegstein, 2010). Brain-derived neurotrophic factor (BDNF) expression, is involved in neuron growth, survival and differentiation in the developing central nervous system (Briones and Woods, 2013; Taschetto Vey et al., 2020). BDNF expression starts around GD 10.5 in rodents and in the 8th post coital week in human embryos (Esvald et al., 2023). Its disruption may impact neurodevelopment of offspring (Fatima et al., 2019; Okano et al., 2023). Between GD 10.5 and 17.5 in the neocortex of mice, RGPs differentiate into neocortical neurons. In humans, this transition occurs between gestational weeks 7 and 27 (Zahr et al., 2019). At GD 13.5, the average cell cycle time for proliferative cells in the ventricular zone is approximately 12 h, with the S-phase (DNA synthesis phase) lasting around 6 h in mice (Hoshino et al., 1973; Schmahl, 1983; Takahashi et al., 1995). This cell cycle length is comparable in adult mouse models (Hayes and Nowakowski, 2002). However, it may differ *in vitro* depending on the cell culture micro-environment. For example, the balance between oxidation and reduction is crucial for neurogenesis, neuronal migration, synaptogenesis and pruning (Londono Tobon et al., 2016). Silencing the glutathione peroxidase (whose function is to reduce hydrogen peroxide and lipid hydroperoxide in physiological context) during embryogenesis leads to impaired hindbrain development and cerebral apoptosis (Borchert et al., 2006).

In the rat brain most synapses are formed between birth (postnatal day, PND, 0) and PND 21. Synaptogenesis peaks around PND 14. The precise timeline depends on the specific brain regions (Semple et al., 2013). In children, synaptogenesis peaks around one to two years (Zeiss, 2021). In the presynaptic bouton, synaptic vesicles store excitatory (glutamate) or inhibitory (gamma-aminobutyric acid), GABA neurotransmitters or modulators. Key proteins like Bassoon, an active zone matrix proteins, contributes to neurotransmitters release in the synaptic cleft and synaptic transmission (Ackermann et al., 2015). In inhibitory synapses, the postsynaptic bouton will express GABA or glycinergic receptors on their membrane surface, stabilized by the protein gephyrin (Groeneweg et al., 2018; Dos Reis et al., 2022). In excitatory synapses, the post-synaptic bouton will express glutamatergic, N-Methyl-D-aspartic acid (NMDA), Aminomethylphosphonic acid (AMPA) and potassium receptors on their membrane surface, stabilized by the post-synaptic density protein 95 (PSD-95) (Kim and Sheng, 2004). The balance between excitatory and inhibitory synapses at the protein level with Gephyrin and PSD-95 in developing synapses (Keith and El-Husseini, 2008) is crucial for the stabilization of neuronal circuits (Monday et al., 2018). The inhibitory activity of synapses is required to refine the optimal neural representation from many competing inputs that increasingly stimulate the developing brain (Peerboom and Wierenga, 2021). Interestingly, cell loss in the hippocampus following seizures has been associated with an increase in GABAergic synapses (Knuesel et al., 2001). Disruptions in this equilibrium can result in neurodevelopmental disorders such as autism spectrum disorders (Bozzi et al., 2018; Antoine et al., 2019; Sohal and Rubenstein, 2019). Indeed, these distinct stages of neurodevelopment have been shown to be altered after low level RF-EMF exposure.

In adult rodent brain, NSCs are involved in the neurogenesis that occurs in two neurogenic zones: the subgranular zone of the hippocampal dentate gyrus and the subventricular zone (SVZ) of the lateral ventricles (Abrous et al., 2005). The SVZ NSCs are multipotent B1 cells produced during embryonic phase. B1 cells can give rise to transit-amplifying neural progenitor cells (C cells) that in turn generate migrating neuroblasts (A cells) (Alvarez-Buylla and Lim, 2004). B1 cells can differentiate into astrocytes, oligodendrocytes, ependymal cells (E cells) and neurons (Menn et al., 2006; Ortega et al., 2013).

The study of the alteration of the oxidative stress balance has been a major focus after RF-EMF exposure (Schuermann and Mevissen, 2021)

as a potential key event in the neurotoxicity pathway (Nishimura et al., 2021). Following chronic 2450 MHz exposure from pregnancy to PND 21, 1 h per day at 0.1 W/kg, lipid peroxidation was higher and glutathione peroxidase was lower in rats (Çelik et al., 2016). A reduction in pyramidal neurons in the Ammon's horn (CA) in PND 56 rats was observed following 900 MHz at 0.024 W/kg exposure for 1 h each day (Şahin et al., 2015), or chronic exposure to 835 MHz at 1.6 W/kg daily in adult mice (Maskey et al., 2010) with 30 days of exposure for both experiments. At PND 28, chronic exposure to 900 MHz at 1.15 W/kg for 1 h daily over 28 days of rats induced neuronal loss and cellular architecture disruption (dendritic intersection and branching point) was also noted in the amygdala (Narayanan et al., 2018). In adult rats, increased oxidative stress and histological changes in the hippocampus and cerebellum after 1800 MHz at 0.6 W/kg for 2 h daily over 3 months were showed (Hussein et al., 2016). *In vitro*, after 900 MHz RF-exposure at 2.287 W/kg, neurospheres showed a decrease in number and size and in percentage of differentiation into neurons (Eghlidospour et al., 2017).

Regarding RF-EMF exposure implications at the synaptic level, only *in vivo* studies were performed in adult mice model. A decrease in the expression of vesicular trafficking regulators, synapsin I and synapsin II, in cortical neurons was observed (Kim et al., 2017). With the same exposure extended to 12 weeks, a significant reduction in the number of synaptic vesicles and dopaminergic neurons in the striatum of exposed rats was noted (Kim et al., 2019). A significant reduction in dendritic spines was shown in the dentate gyrus of the hippocampus in mice exposed to 835 MHz RF at 4 W/kg for 5 h daily from PND 1 over 4 weeks (Kim et al., 2021). For *in vitro* studies, a significant difference was shown on neurite outgrowth following NSCs exposure to 1800 MHz RF at 4 W/kg field for 3 days but not for 1 W/kg and 2 W/kg exposure (Chen et al., 2015). At 900 MHz, Del Vecchio et al., (2009) showed different results with a reduction in the number of neurites in murine cell line and in rats' cortical primary neurons with decreased beta-thymosin mRNA. In terms of synaptic impact, a decreased number and length of branches of a primary culture of cortical neurons after being exposed to 1800 MHz at 4 W/kg 1 h per day from day *in vitro* 1 (DIV) to DIV 4 was reported by Su et al., (2018). Further investigation is warranted on developmental biology to ascertain the absence of biological effect or sanitary risk below RF-EMF ICNIRP thresholds for neonates, juveniles and adolescents. Our study is the first to assess similar key events of neurodevelopment following *in vivo* GD 8 to PND 17 900 MHz exposure at regulatory limits or following DIV 1 to DIV 10 *in vitro* 900 MHz exposure.

The objective of this research was to further investigate the hypothesis that 900 MHz RF-EMF exposures at whole-body (wb) SARs corresponding to ICNIRP limits for humans may modify progeny neurodevelopment on proteomic profile at PND 0, cellular proliferation, synaptogenesis, and micro-environment at PND 8 and PND 17. Here we aimed to fulfil both *in vivo* and *in vitro* approaches by assessing 900 MHz at public limits on the key cellular events of neurodevelopment.

2. Materials and methods

2.1. Rats

Protocols were approved by the Regional Ethical Committee (CRE-MEAP N. 96) and the French Ministry of Research (APAFIS#19003, 26/08/2019; Bodin et al., 2024). Twenty-seven pregnant female rats (Sprague Dawley, 10–12 weeks old; Janvier (France) were received at the vivarium at GD 3 and had 5 days in their exposure chambers to acclimatize (12 h light/dark cycle (light intensity: 300 lux) at 22°C room temperature (RT)).

2.2. *In vivo* procedures and experimental groups

The experimental design is summarized in Fig. 1. Pregnant Sprague Dawley rats were randomly divided into three groups: a sham control

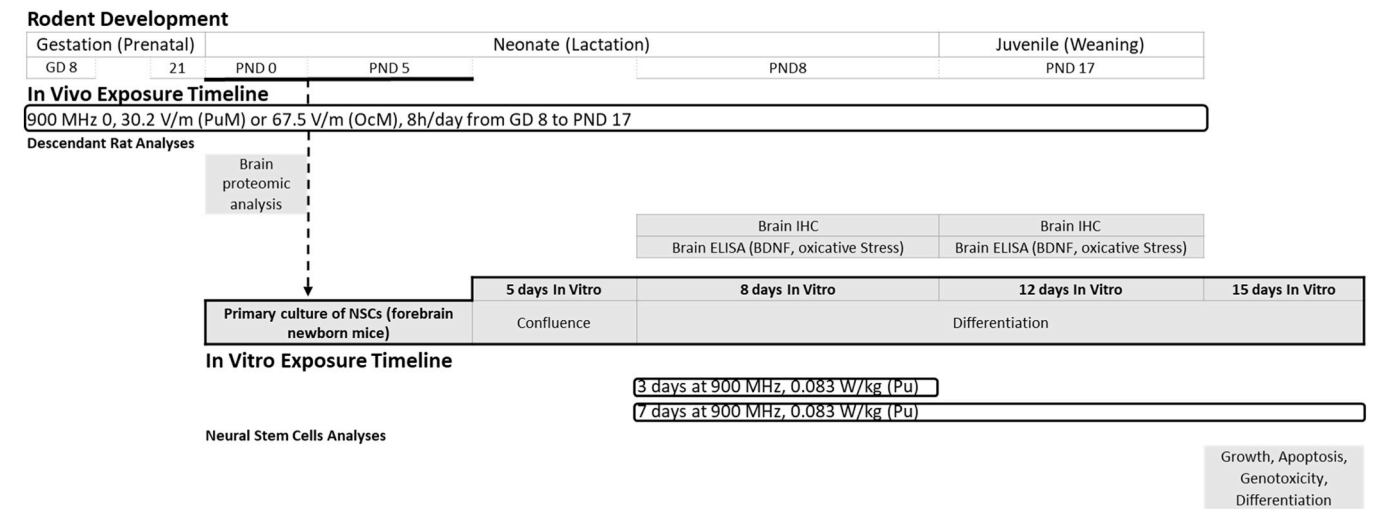


Fig. (1). Design of gestational, post-natal and *in vitro* RF exposure and endpoint assessment. Daily exposures from 11:00–19:00 h starting at GD 8 and until PND 17 were performed. The wbsAR was 0 (sham-exposed group), 0.08 W/kg (PuM group) or 0.4 W/kg (OcM group). Proteomic analysis was performed at PND 0, immunohistochemistry and ELISA tests on BDNF and oxidative stress were performed at PND 8 and PND 17 on male pups' brains. The neural stem cells were exposed for 3 days or 7 days to 900 MHz RF at 0.08 W/kg (the RF limit for the public; Public (Pu) group). Cells viability, differentiation and proliferation were assessed after 10 days. RF: radiofrequency; GD: gestational day; PND: postnatal day; SAR: specific absorption rate; PuM: general public whole body (wb) SAR for mothers; OcM: occupational wbsAR for mothers; Pu: group of cells exposed at the SAR corresponding to the general public limit.

group (n = 9), the public exposure group (PuM, n = 8), and the occupational exposure group (OcM, n = 8). Both the PuM and OcM groups were exposed to 900 MHz continuous-wave RF-EMF for 8 h daily from GD 8 to PND 17. The PuM group was exposed to a field strength of 30.2 V/m, resulting in a whole-body specific absorption rate (wbsAR) of 0.08 W/kg in pregnant rats, while the OcM group received 67.5 V/m, corresponding to a wbsAR of 0.4 W/kg in pregnant rats. The sham group underwent the same procedure without RF exposure (field strength near environmental baseline). The experimental protocol has been described previously (Bodin et al., 2024). Litters were standardized at birth to include 3 males and 3 females. For this study, two pups (one male and one female) were semi-randomly selected for sacrifice on PND 8 and PND 17. Rats were given intraperitoneal injections of 5'-bromo-2'-deoxyuridine (BrdU), 50 mg/kg, 2 h before euthanasia. The aim was to mark newly synthesized DNA. RF-EMF exposures were conducted in reverberation chambers, with exposure specifics previously reported by Capstick et al. (2017) and Bodin et al. (2024).

2.3. Proteomic in neonats' brain

Brains were harvested from surplus male pups at PND 0. The brain areas from cortex region and hippocampal region were then dissected using a micro-punch technique (3 pups per litter). Proteins were extracted and digested from 30 mg of ground tissue using IST-NHS sample preparation kit (Preomics, Planegg (Martinsried), Germany) using manufacturer's recommendations. Differential proteomic analysis was performed using tandem mass tags (TMT) for relative quantitative proteomic analysis. The labelled samples were then mixed and analyzed in a single liquid chromatography-mass spectrometry (LC-MS) experiment. Samples treated in this way were then fractionated using the High pH reversed-Phase kit according to the supplier's recommendations.

The fractioned samples were injected, separated on a nano-HPLC system (RSLC NCS-3500 RS/WPS 3000). A binary gradient of aqueous solvent (water/0.1 % formic acid (V/V)) and organic solvent (acetonitrile/0.1 % (V/V) formic acid) at a flow rate of 300 nl/min was used following the gradient of 170 min. These experiments were performed on three biological replicates. The mass spectrometry (MS) and MS/MS obtained were analyzed using Proteome Discoverer 2.5 by querying the Trembl *Rattus norvegicus* database with a false positive rate of less than 0.01 based on a search of the database and the reverse database. The

MS/MS data (raw data, identification and quantification results) are available to ProteomeXchange Consortium (<http://www.proteomexchange.org> accessed on 9th July 2024) via the PRIDE partner repository with dataset identifier PXD053803. The sequences were compared to find sequence homology (protein sequence from GenBank).

2.4. Preparation of tissue from juvenile rats' brain

The brains were separated into 2 hemispheres. One half was cut to obtain brain sections of 300 µm and frozen in isopentane cooled to -50°C. It was stored at -80°C until dissection using the "micro-punch" technique (Palkovits, 1973) for BDNF and oxidative stress markers ELISA. The other half was post-fixed in paraformaldehyde (PFA) 4 % (diluted in 0.1 M phosphate buffer, pH 7.4) for approximately 24 h in the fridge at 4°C. The brains were then placed in 0.1 M phosphate buffer (pH 7.4) containing 30 % sucrose (a volume of approximately 30 mL per vial) at 4°C for the required time for the brain to sink to the bottom of the vial (24 h to 48 h). They were stored in the freezer at -80°C until being sectioned in the cryostat. Slices were cut in sagittal plane of 14 µm in size and mounted on superfrost plus slides. The sections were stored at -20°C until BrdU immunohistochemistry.

2.5. BrdU/DAPI immunohistochemistry staining

Superfrost plus slides with brain slices were placed in an incubator at 37°C for 30 min to dry. Slides were rehydrated in HBSS 1X bath under agitation at RT. All the slides were placed in a 1 M HCL vat in a water bath at 37°C for 30 min to denature the DNA. The process was stopped with washes in ice cold 1X HBSS. The sections were incubated with 0.3 % Triton X-100 with 2 % goat serum diluted in HBSS 1X solution at RT for 1 h. Each slice of brain was then surrounded with a hydrophobic pen to perform sequential staining with 150 µL of blocking solution containing anti-BrdU monoclonal antibody (1/200, B2531, Sigma-Aldrich). They were incubated over night at 4°C. Washing steps were performed before adding the secondary antibody (1/200, A21202, Thermofisher) 2 h at RT. DAPI staining at 1/2000 was performed for 15 min at RT. Sections were washed and coverslipped in fluorescent mounting medium (fluoromount) and stored at 4°C for later observation under confocal microscope.

2.6. Bassoon - gephyrin - PSD-95 immunofluorescence

Superfrost plus slides with brain slices were placed in an incubator at 37°C for 30 min to dry. They were then rehydrated in HBSS 1X bath under agitation at RT. Put in a bath of saturation buffer with 10 % goat serum, 0.5 % Triton-100X in TBS 1X at RT on rotating grid for 1 h. Each brain slice was then surrounded with a hydrophobic pen to perform sequential staining with 150 µL of blocking solution with rabbit anti-Bassoon (Synaptic System, 141003, 1/500), guinea pig anti-gephyrin (Synaptic System, 147318, 1/200) and mouse anti-PSD-95 (Abcam, ab2723, 1/500). They were put under agitation at 4°C overnight. After washing with TBS 1X, secondary antibodies (1/200) were added with 0.05 % Tween in TBS 1X under agitation 2 h in dark. Sections were washed and coverslipped in fluorescent mounting medium (fluoromount) and stored at 4°C for later observation under confocal microscope.

2.7. Confocal imaging

A laser scanning confocal microscope was used: Olympus Fluoview 1000. The number of BrdU-positive and DAPI-positive cells were counted in each three sagittal sections (spaced 1 µm apart) per brain in regions of interest (ROI). Results were recorded as the average number of BrdU⁺DAPI⁺ cells per section and per cm². Densities were measured by Image J software.

The quantification of inhibitory synapses and excitatory synapses was made with colocalization of immunofluorescence of gephyrin/bassoon or PSD95/bassoon antibody, respectively. The quantification was performed on confocal images (x600) with an automatic probability-principled synapse detection algorithm in the Fiji plug-in of ImageJ: SynQuant (Wang et al., 2020).

2.8. BDNF quantification by electrochemiluminescent immunoassay

The singleplex assay that measured BDNF levels was provided by Meso Scale Discovery (MSD; Gaithersburg, MD, USA). The hippocampal and cortex regions of the brain were sampled with a micropunch (3 µm) on a sagittal plane. The quantity of BDNF was then measured using MSD protocol (U-PLEX Rat BDNF Assay K1536WK-1) and analysed with Methodicalmind software.

2.9. Detection of oxidative stress with ELISA

Oxidative stress markers were measured on lysate of the whole brain normalized at 12.5 mg per mL. Lipid peroxidation was determined with MDA ELISA kit (Sigma-Aldrich-MAK085- St.Louis, MO, USA) and the results were expressed as nmol/mL. The total antioxidant capacity (TAC) was measured using a colorimetric ELISA kit (Abcam, Cambridge, UK; ab65329). TAC was calculated using a standard curve, and results were expressed as antioxidant concentration (nmol/mL). 8-hydroxy-2'-deoxyguanosine (8-OHdG) Rat ELISA kit (Abcam, Cambridge, UK; ab285302) was used according to the manufacturer's protocol.

2.10. Mice

Janvier Labs provided the breeding adult C57BL/6JRj mice (Le Genest-St-Isle, France), and standard conditions were maintained with *ad libitum* access to water, food, and 12-hour light/dark cycles.

2.11. In vitro primary culture of NSCs of newborn mice

In vitro murine primary NSC cultures were performed on PND 1 to PND 5 C57BL/6JRj mice and NSCs were cultured according to the modified experimental procedures of Delgehyr et al., (2015). Briefly, newborn mice were sacrificed by decapitation, and brains were transferred to a Petri dish containing cold complemented Hank's solution.

The olfactory bulbs and hippocampal have been detached while the telencephalon surface was detachable by peeling off the meninges. The dissected telencephalon was mechanically dissociated followed with the add of 1 mL of the enzymatic digestion solution per tube. After an incubation of 45 min at 37 °C, 5 % CO₂, samples were centrifuged for 1 min at 110 g (4 °C), and 1 mL of the stop solution was added per tube. After a centrifugation (1 min 110 g 4 °C), the cells were rinsed with 5 mL of L15 medium. The cells were centrifuged for 5 min at 110 g 4 °C and were suspended mechanically in 1 mL of the NSCs growth medium. The cells were plated into poly-L-Lysine precoated 25 cm² flasks (one brain per flask).

2.12. In vitro exposure and field measurements

For all experiments, NSCs were exposed with a GSM 900-MHz mobile simulator in a "GSM-like" (1/8 Duty-cycle 216 Hz). The main concept of the system is based on the wire patch cell (WPC) *in vitro* exposure system developed by XLIM according to publication Laval et al., (2000). During exposure, the temperature of the incubator was monitored and maintained at 37 ± 0.1°C.

The amplifier provided 0.16 W for SAR 0.08 W/kg (general public limit SAR for cells, Pu). The maximum power used (0.16 W) was about 200 times lower than the power inducing a 0.2 degrees temperature increase, i.e., 31.6 W. Finite Difference Time Domain technique and experimental investigations have been used concomitantly to design the cell at 900 MHz. The numerical dosimetry was validated by dosimetry measurements. These investigations estimated the dosimetry precision at 11 %. SAR was calculated as followed: $SAR = \sigma |E|^2 / \rho$ (E is the root-mean-square local electric field strength (V/m), σ the effective conductivity (S/m), and ρ the aqueous sample density (kg/m³). In the model, cells were continuously exposed for 3 or 7 days either at 0 W/kg or at 0.083 W/kg SAR. The averaged SAR calculated for this experiment was 0.08 W/kg (general public limit SAR, Pu).

2.13. In vitro cell differentiation

When the cells reached confluence, usually 5 days after plating, the flasks were shaken at 250 rpm overnight at RT, to remove differentiated cells. The next day, the flasks were rinsed with sterile Ca²⁺ + /Mg²⁺ + free Dulbecco's phosphate-buffered saline (DPBS, SIGMA D8537). One mL of 0.05 % Trypsin-EDTA (1X, GIBCO 25300-054) was added to each flask to remove cells, and flasks were incubated for under 15 min. After shaking briefly, the cells came to the surface, and 1 mL of NCS growth medium was added. The cells were centrifuged for 7 min at 110 g 4 °C, then suspended at high density (1–2.10⁶ cells/mL or 2.10⁵ cells per 20 µL for immunocytochemistry). Up to 6 cell suspensions should be grouped together to avoid the individual effect. The 35 mm Petri dishes were incubated for 30 min in a cell incubator (37 °C 5 % CO₂) to provide cell adhesion at high density before adding 3 mL of NSC growth medium. The NSC growth medium was used for less than 7 days *in vitro* (DIV) to initiate spontaneous differentiation into neuroglial cells. The medium was removed every two days.

2.14. In vitro cell viability

Cell viability was assessed using tetrazolium dye 3-(4, 5-dimethylthiazol-2-yl)2, 5diphenyl-2H-tetrazolium bromide (5 mg/mL MTT) according to the manufacturer's instructions (Vybrant® MTT Cell Proliferation Assay Kit, ThermoFisher Scientific). Cells were plated onto PLL precoated 35 mm Petri Dishes and exposed. Petri dishes were rinsed with HBSS and the MTT was added to the medium (12 mM stock solution). After 4 h of incubation at 37 °C and 5 % CO₂, the medium was removed, and the formazan end-product was solubilized in SDS-HCl. After 2 h at 37 °C and 5 % CO₂, formazan production was determined by spectrophotometry (CLARIOstar, BMG LABTECH) at a wavelength of 562 nm.

Triplicate evaluation was conducted on every sample, with each triplicate representing a pool of up to six individual suspension NSC-derived cultures. Three experiments were carried out independently for each condition.

2.15. *In vitro* TUNEL assays

TUNEL assays were conducted with an ApopTag® fluorescein in situ Apoptosis Detection Kit (Chemicon S7110) following the indicated protocol. The number of apoptotic cells and number of total nuclei were counted.

2.16. *In vitro* immunocytochemistry

Cell genotoxicity, proliferation and differentiation were analysed by immunocytochemistry. NSCs were plated at a concentration of 2.105 cells per 20 μ L into 35 mm Petri dishes containing 4 PLL precoated coverslips. Cell genotoxicity was performed at the end of the exposure period (D3 and D7). Cell differentiation was realized at day 10. Proliferation was evaluated at the end of the exposure period and at day 10. The medium was removed, and the coverslips were washed with Tris-Buffer Saline 1X (TBS, pH 7.6, Tris-HCl 50 mM, NaCl 150 mM), fixed with 4 % paraformaldehyde (PFA) for 10 min at RT. After washing, cells were permeabilized with 10 % FBS; 0.20 % Triton X-100 (Euromedex, ref 2000A) and 2 % Bovine Serum Albumin (BSA Fraction V, ICN Biomedicals, ref 9048–46–8) for 15 min at RT. Coverslips were then incubated overnight at RT using the following primary antibodies: anti-Ki-67 (1:500, polyclonal IgG rabbit, ABCAM ab15580) for cell proliferation; anti-Nestin (1:500, monoclonal IgG1k mouse, ABCAM ab11306) for B1 and C cells; anti-GFAP (1:500, monoclonal IgG1 mouse, SIGMA G3893 or 1:500, polyclonal IgG rabbit, Dako Z0334) for B1 cells and astrocytes, and anti-Olig2 (1:500, polyclonal IgG rabbit, Millipore AB9610) for oligodendrocyte precursor cells. Coverslips were rinsed with TBS1X and incubated with the appropriate secondary antibodies (anti-rabbit, anti-mouse, or anti-rat Ig G Alexa-488 or TRITC conjugated) for 45 min at RT in 2 % BSA and 10 % FBS solution. After another washing step DAPI was used to stain the nuclei of cells. Coverslips were mounted on glass slides in the Fluoromount-G (SouthernBiotech). Microscopic images were produced by using a fluorescent microscope (Leica DM6000B) with immersed 40x magnification and analyzed with Metamorph® software.

Cell growth was analysed at the end of exposure times (day 3 and 7) and on day 10 by measuring the total number of nuclei in Pu exposed cells in comparison to the sham treated cultures. To assess the effect on cell proliferation and apoptosis, Ki-67-positive cells and Apoptag-positive cells were counted respectively on day 3, 7 and/or 10. To assess the effect of Pu exposure on DNA double strand breaks, the number of cells with DNA double strand breaks were counted at the end of time exposure.

Quantitative analysis of double immunostaining was performed for each experimental condition using four wells per condition. For each coverslip, 5–6 representative microscopic fields were randomly acquired at 40 \times oil immersion magnification with the Leica DM6000B microscope. Images were analysed with ImageJ® software, where the total number of nuclei (DAPI-stained) and the number of single- or double-labelled cells were manually counted. On average, each field contained approximately 150 cells, corresponding to 750–900 cells analysed per coverslip. Data from all fields of a coverslip were averaged to obtain one value per well, and the four wells of the same condition were then averaged to yield a single value per condition. Results are expressed as the percentage of positive or double-positive cells relative to the sham group.

2.17. Statistical analysis

For proteomic data, principal component analysis (PCA) and differential expression analysis, were performed with Proteome Discoverer

2.5 (Thermo Fisher Scientific Inc. USA). Means \pm standard error was analysed using GraphPad Prism (Version 8.0.2, GraphPad Software, Boston, 166 Massachusetts USA). Statistical significance was set for p values lower than 0.05 in all statistical test.

To compare more than two groups of quantitative data (the SAR effect on the sham, 0.08 and 0.4 W/kg groups, the time (age) effect or the slice effect), a mixed-effects model was used to analyse the significance of our three factors and the interaction between each factor. A mixed effect was used subsequently to analyse interactions. When mixed effects were significant, Sidak's or Turkey's t test post hoc were conducted.

To compare two groups of quantitative data (sham versus RF-EMF exposed groups in *in vitro* approach), all datasets were refined with the ROUT outlier test (Q=5 %) to identify values to exclude. Mann-Whitney test was realised for testing and each mean was compared with the sham control group mean.

3. Results

3.1. Distinct proteomic profiles between sham and RF-EMF exposed groups at PND 0

Proteomic analysis revealed considerable heterogeneity across samples between the four individuals inside each group, the different conditions (Sham, PuM and OcM), and the brain areas (Hippocampus, Cortex). The volcano plots (Fig. 2) for the four separate comparisons with the sham group (Cortex PuM and OcM, Hippocampus PuM and OcM) show a total of 10 differentially expressed proteins.

The PCA (Fig. 3) allows the transformation of possibly correlated values into principal components that best represent their variances. The aim is to reduce the number of dimensions that will describe proteins dynamics. In our analysis, the first two principal components, which together explain 55 % of the total variance, capture the main differences in protein expression across samples. The PCA clearly separates the Sham and exposed groups, suggesting that exposure leads to coordinated changes in protein expression. The observed clustering indicates that specific groups of proteins could be expressed differentially in response to exposure.

There are few statistically significant changes in the protein expression due to the RF-EMF exposure. The different proteins that are differentially expressed and that could be extracted from the analyses are presented in Table 1. The dihydropyrimidinase-related protein 1 (DRP1; primary accession number: Q62950; Fig. 2; Table 1) level was decreased in both PuM group in cortex (Ratio: 0.445) and hippocampus (Ratio: 0.445) areas but also in OcM group in the hippocampus area (Ratio 0.488) compared to sham groups.

The Plexin A4 protein level (primary accession number: D3ZES7; Fig. 2; Table 1) was increased in both PuM group in the cortex area (Ratio: 1.653) and OcM group in the cortex (Ratio: 2.217) and hippocampus area (Ratio: 2.217) compared to sham group.

The "Similar to RIKEN cDNA" (primary accession number: F7F776; Fig. 2; Table 1) also showed increased levels in PuM group in cortex area (Ratio: 2.028) and in OcM group in cortex (2.135) and hippocampus area (2.305) compared to sham groups. The sequence was homologous with the protein BAP18.

Some proteins have also been differentially expressed but only in one group. The Elongin-C (Ratio: 0.375), Ncam1 protein (Ratio: 2.574) and Heterogenous nuclear ribonucleoprotein D (Ratio: 2.718) were increased in the cortex PuM group. In the cortex OcM group only, zero beta-globin (0.425), Superoxide dismutase (SOD; Ratio: 0.445) and small nuclear ribonucleoprotein E (Ratio: 2.574) were respectively decreased and increased. In the hippocampus OcM group only, the vacuolar protein sorting-associated protein 45 (VPS45; Ratio: 0.368) was decreased.

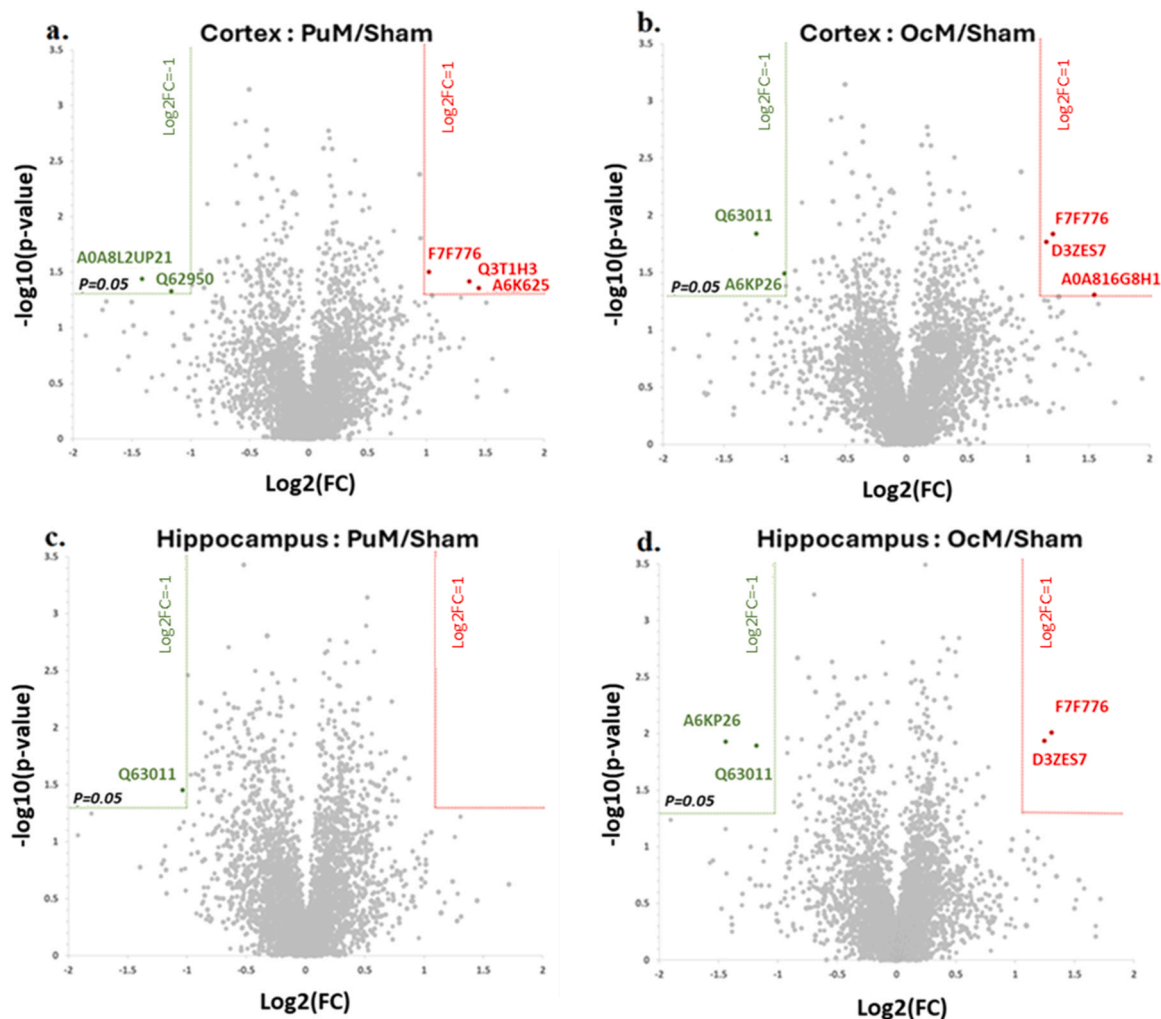


Fig. (2). Overall distribution of differentially expressed proteins of rat brain samples from cortex or hippocampus region ($n = 4$). The differentially expressed proteins ($p < 0.05$) are represented with volcano plots between each two groups (a) Cortex: PuM/Sham, (b) Cortex: OcM/Sham, (c) Hippocampus: PuM/Sham, (d) Hippocampus: OcM/Sham. The primary accession identification (UniProt) is given for significant differentially expressed proteins. PuM: general public whole body (wb) SAR for mothers; OcM: occupational wbSAR for mothers.

3.2. Effect of RF-EMF on hippocampal BdnF and BrdU+ cells at PND 8 and PND 17

For the hippocampus, the BDNF level of the male pups at PND 8 and PND 17 is presented in Fig. 4a. The results indicate that there was a significant difference in BDNF level between treatments (p -value = 0.0193) and between ages (p -value = 0.001) but no interaction. This difference was refined using complementary multiple t -test analysis showing a tendency to increase between Sham and PuM groups at PND 8 (adjusted p -value = 0.0528) and PND 17 (adjusted p -value = 0.0596) but not significant. BDNF levels increased with age in sham (p -value = 0.0247) and PuM groups (p -value = 0.0458) but not in OcM group.

The quantification of BrdU+ cells in the dentate gyrus of the male pups at PND 8 and PND 17 is presented in Fig. 4b. No significant effect on BrdU+ cells between treatments, slice area or interaction between factors was shown. A significant decrease with age was shown (p -value < 0.0001) confirmed by multiple t -test analysis in all groups.

3.3. Effect of RF-EMF on hippocampal synaptogenesis at PND 8 and PND 17

The total number of synapses in the dentate gyrus of the male pups at PND 8 and PND 17 is shown in Fig. 5a. The results of the mixed-effects

analysis with age and treatment show significant differences between groups for age (p -value < 0.0001), treatment (p -value = 0.0120) and interaction (p -value = 0.0429). This difference was refined using complementary multiple t -test analysis showing significant decrease between sham and PuM group (adjusted p -value = 0.0061) and between sham and OcM (adjusted p -value = 0.0026) at PND 8. No significant difference was found at PND 17 for both groups. Complementary multiple t test showed also significant decrease between PND 8 and PND 17 for sham group (adjusted p -value < 0.0001), OcM group (adjusted p -value < 0.0001) and PuM groups (adjusted p -value = 0.0056).

Synapse balance in the dentate gyrus of the male pups at PND 8 and PND 17 is shown in Fig. 5b. The result shows a significant effect of age (p -value < 0.0001) and interaction between age and treatments (p -value = 0.0359) but no effect of treatment. This difference was refined using complementary multiple t -test analysis showing significant decrease between sham and OcM groups (adjusted p -value = 0.0266) but also between sham and PuM groups (adjusted p -value = 0.0241) at PND 8. No effect of treatments was found at PND 17 between groups. Complementary multiple t test showed also significant differences between PND 8 and PND 17 for sham group (adjusted p -value = 0.0002) and OcM (adjusted p -value = 0.0313) but not for PuM group.

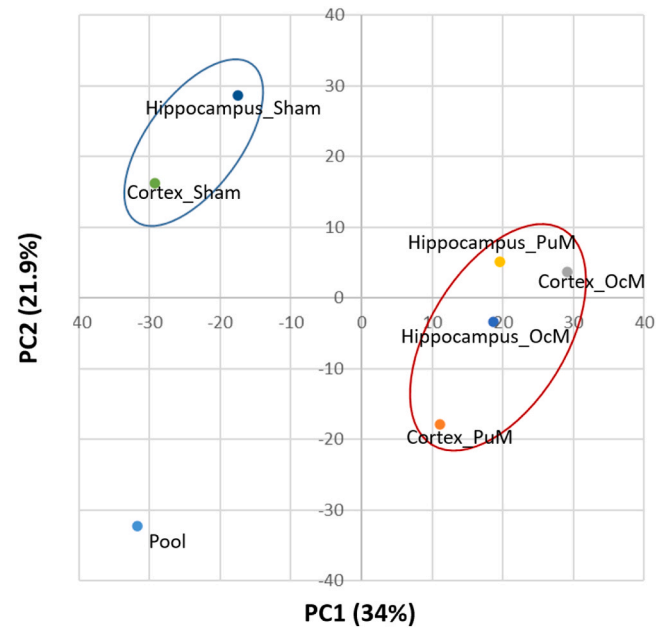


Fig. (3). Principal component analysis (PCA) biplot of rat brain samples from cortex or hippocampus region with sham, PuM and OcM exposed groups (n = 4). The first two axes accounted for 55 % of variance and show a clear distinction between proteomic profiles of Sham and exposed groups. PuM: general public whole body (wb) SAR for mothers; OcM: occupational whole body wbSAR for mothers; PC1: first principal component (PC1); PC2: second principal component.

3.4. Effect of RF-EMF on cortical BrdU+ cells at PND 8 and PND 17

For the cortex, the BDNF level of the male pups at PND 8 and PND 17 is shown in Fig. 6a. The results indicated significant effect of age (p-value < 0.0001), treatment (p-value = 0.0065), and interaction between age and treatment (p-value = 0.0242) for PuM group. For OcM group, the results indicated significant effect of age (p-value < 0.0001), treatment (p-value < 0.0001) and interaction between age and treatment (p-value < 0.0001). The results suggested that there was significant effect for treatments (p-value = 0.0065) and age (p-value < 0.0001) but no effect for interaction. This difference was refined using complementary multiple t-test analysis showing significant decrease for PuM (adjusted p-value = 0.0004) and OcM (adjusted p-value = 0.0238) groups only at PND17 but no effect at PND 8. Significant effect of age was also found for sham group (adjusted p-value < 0.0001), PuM group (adjusted p-value < 0.0001) and OcM group (adjusted p-value < 0.0001).

The BrdU+ cells in the cortex of the male pups at PND 8 and PND 17 is shown in Fig. 6b. The results suggested that there was a significant decrease of BrdU+ cells between treatments (p-value = 0.0312), with age (p-value < 0.0001) and interaction between age and treatment (p-value = 0.0261). The results suggested that there was a significant decrease of BrdU+ cells between treatments (p-value = 0.0202), with age (p-value < 0.0001) and interaction between age and treatment (p-value = 0.0151). These analyses with age and treatment showed a significant effect of age (p-value < 0.0001), treatment (p-value = 0.0465) and their interaction (p-value = 0.0248). This difference was refined using complementary multiple t test analysis showing significant decreased at PND 8 between the sham group and both the OcM group (adjusted p-value = 0.0016) and PuM group (adjusted p-value = 0.0466) but no significant difference at PND 17. Significant effect of age was also found for sham group (adjusted p-value < 0.0001), PuM group (adjusted p-value = 0.0015) and OcM group (adjusted p-value = 0.0099).

Table (1)

Proteins differentially expressed in proteomics from brains of pups at PND 0 (n = 4). The primary accession identification (UniProt) is given for significant proteins. PuM: general public whole body (wb) SAR for mothers; OcM: occupational whole body wbSAR for mothers; OS: origin species; OX: organism identifier; GN: gene name; PE: protein existence; SV: sequence version.

Comparison Cortex_PuM / Cortex_Sham			
Accession	Description	Abundance Ratio	Abundance Ratio P-Value
A0A8L2UP21	Elongin-C, OS=Rattus norvegicus, OX= 10116, GN=Eloccl4, PE= 3, SV= 1,	0.375	4.71E-02
Q62950	Dihydropyrimidinase-related protein 1, OS=Rattus norvegicus, OX= 10116, GN=Crmp1, PE= 1, SV= 1,	0.445	3.68EE-02
F7F776	Similar to RIKEN cDNA 1110020A23, OS=Rattus norvegicus, OX= 10116, GN=C10h17orf49, PE= 1, SV= 1,	2.028	3.10E-02
Q3T1H3	Ncam1 protein, OS=Rattus norvegicus, OX= 10116, GN=Ncam1, PE= 2, SV= 1	2.574	3.85E-02
A6K625	Heterogenous nuclear ribonucleoprotein D, isoform CRA_d, OS=Rattus norvegicus, OX= 10116, GN=Hnrmnpd, PE= 4 SV= 1	2.718	4.36E-02
Comparison Cortex_OcM / Cortex_Sham			
Accession	Description	Abundance Ratio	Abundance Ratio P-Value
Q63011	Zero beta-globin (Fragment), OS=Rattus norvegicus, OX= 10116, PE= 3, SV= 1,	0.425	2.84E-02
A6KP26	Superoxide dismutase, OS=Rattus norvegicus, OX= 10116, GN=Sod2, PE= 3, SV= 1,	0.445	3.22E-02
D3ZES7	Plexin A4, OS=Rattus norvegicus, OX= 10116, GN=Plxna4, PE= 3, SV= 1,	2.028	1.71E-02
A0A8I6G8H1	Small nuclear ribunucleoprotein E, OS=Rattus norvegicus, OX= 10116, GN=Snrpe, PE= 3, SV= 1,	2.574	4.12E-02
F7F776	Similar to RIKEN cDNA 1110020A23, OS=Rattus norvegicus, OX= 10116, GN=C10h17orf49, PE= 1, SV= 1	2.718	1.48E-02
Comparison Hippocampus_PuM / Hippocampus_Sham			
Accession	Description	Abundance Ratio	Abundance Ratio P-Value
Q62950	Dihydropyrimidinase-related protein 1, OS=Rattus norvegicus, OX= 10116, GN=Crmp1, PE= 1, SV= 1,	0.445	3.51E-02
Comparison Hippocampus_OcM / Hippocampus_Sham			
Accession	Description	Abundance Ratio	Abundance Ratio P-Value
O08700	Vacuolar protein sorting-associated protein 45, OS=Rattus norvegicus, OX= 10116, GN=Vps45, PE= 1, SV= 1	0.368	1.29E-02
Q62950	Dihydropyrimidinase-related protein 1, OS=Rattus norvegicus, OX= 10116, GN=Crmp1, PE= 1, SV= 1,	0.488	1.30E-02
D3ZES7	Plexin A4, OS=Rattus norvegicus, OX= 10116, GN=Plxna4, PE= 3, SV= 1,	2.217	9.80E-03
F7F776	Similar to RIKEN cDNA 1110020A23, OS=Rattus	2.305	1.20E-02

(continued on next page)

Table (1) (continued)

Comparison Cortex_PuM / Cortex_Sham			
Accession	Description	Abundance Ratio	Abundance Ratio P-Value
	norvegicus, OX= 10116, GN=C10h17orf49, PE= 1, SV= 1,		

3.5. Effect of RF-EMF on cortical synaptogenesis at PND 8 and PND 17

The total number of synapses in the cortex of the male pups at PND 8 and PND 17 is shown in Fig. 6c. The mixed-effects analysis result showed a significant decrease with age ($p\text{-value} < 0.0001$) between PND 8 and PND 17 and a tendency to decrease with treatment ($p\text{-value} = 0.0508$) but no significant interaction between the two. Further analyses confirmed, significant effect of age was found for sham group (adjusted $p\text{-value} = 0.0092$), PuM group (adjusted $p\text{-value} = 0.0054$) and OcM group (adjusted $p\text{-value} = 0.0101$).

The synapses balance (excitation/inhibition) in the cortex of the male pups at PND 8 and PND 17 is shown in Fig. 6d. The result shows a significant effect of age ($p\text{-value} < 0.0001$) and interaction ($p\text{-value} = 0.0115$) but no effect of treatment. This difference was refined using complementary multiple t test analysis showing significant decrease between sham and OcM group only at PND 17 (adjusted $p\text{-value} = 0.0285$). No effect was found at PND 8 or between sham and PuM group at PND 17. The age effect was confirmed with multiple t test analysis, for

sham group (adjusted $p\text{-value} = 0.0065$) and OcM group (adjusted $p\text{-value} < 0.0001$).

3.6. Effect of RF-EMF on oxidative stress at PND 8 and PND 17

The TAC level in the whole brain of PND 8 and PND 17 male pups is shown in Figs. 7a and 8-OHdG level in Fig. 7b. The results suggested that there was no significant difference in 8-OHdG or TAC level between treatments, age, or interaction.

The MDA level in the male pups at PND 8 and PND 17 is shown in Fig. 7c. The results suggested that there was no significant difference in MDA level between treatments or interaction ($p\text{-value} > 0.05$) but a significant difference between ages ($p\text{-value} = 0.0373$). This difference was refined using complementary multiple t test analysis showing no significant between sham, PuM or OcM group.

3.7. Immediately after in vitro 7-day Pu exposure NSCs showed more apoptosis with more Ki-67 + cells and double strand DNA breaks

Data regarding Pu exposure effects on cell growth were reported on Fig. 8a. Total cell number was reduced between the 3-day and 7-day exposures (RF and sham) by a significant culture duration effect ($F_{1,36} = 8.9$ $p = 0.0051$). Pu exposure had no impact on total cell number.

Data regarding Pu exposure effects on cell viability were reported on Fig. 8b. There was no difference due to RF exposure or duration of exposure on the ratio of viable cell number ($SAR F_{1,27} = 0.82$ $p = 0.37$, culture duration $F_{1,27} = 0.15$ $p = 0.69$, $SAR \times$ culture duration

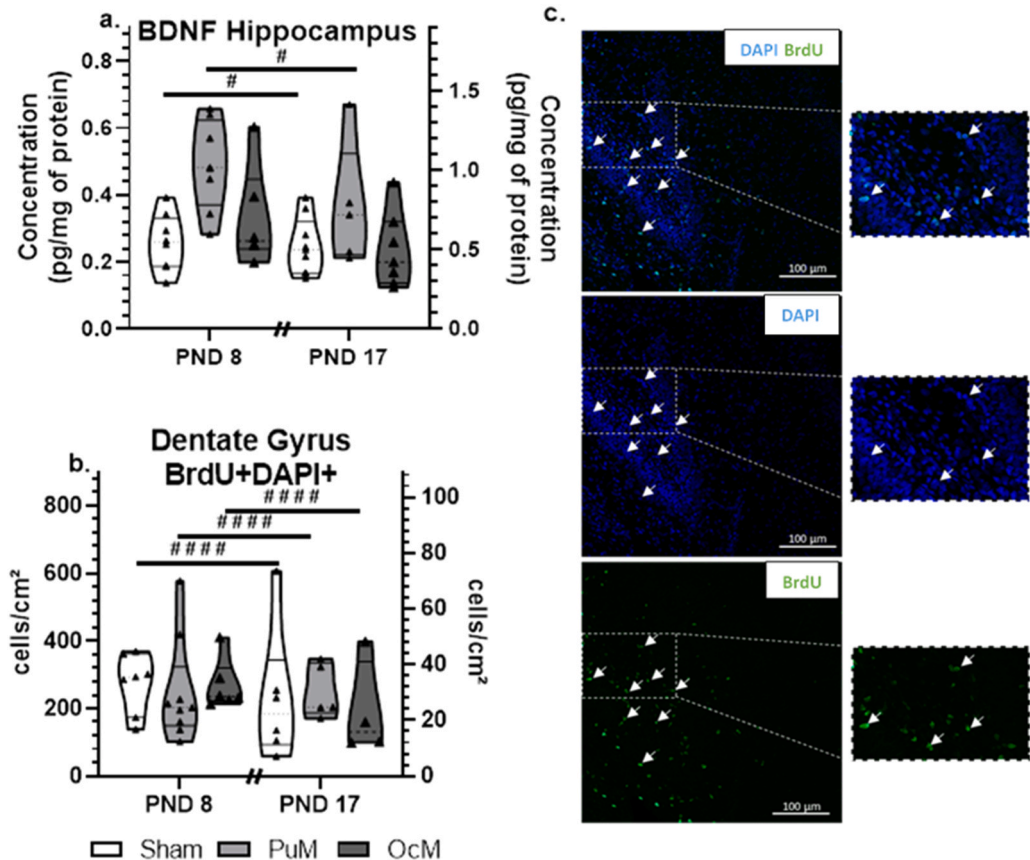


Fig. (4). Effect of RF-exposure from GD 8 to PND 8 or PND 17 on cellular BrdU+ cells and on BDNF levels in the rat hippocampus. (a) There was no RF-EMF effect on BDNF levels but an increase with age for sham and OcM groups. # $p < 0.05$ between ages ($n = 6-8$ per group). (b) BrdU+ cells ($DAPI^+ BrdU^+$) count per cm^2 in the dentate gyrus area. ### $p < 0.001$ between ages ($n = 4-8$ per group). (c) Immunohistochemistry of sagittal brain slices at magnification x20 (scale bar = 100 μm). Cells were immunolabeled for BrdU (green, as indicated by the white arrows) and for DAPI (blue, as indicated by the white arrows). PuM: general public whole body (wb) SAR for mothers; OcM: occupational whole body wbSAR for mothers. The violin plot provides a graphical representation of the distribution of individuals, where the width of the violin at any point reflects the data density. Quartiles are shown with continuous lines and the median is indicated by a dotted line.

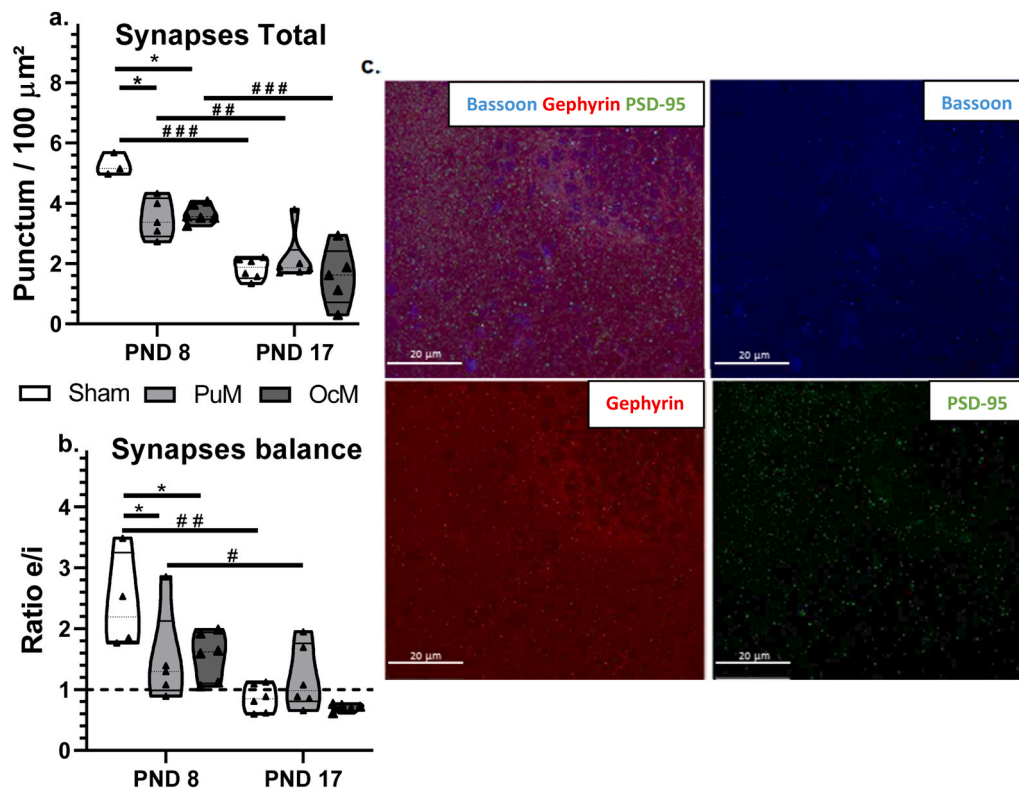


Fig. (5). Effect of RF exposure from GD 8 to PND 8 or PND 17 on synaptogenesis in the rat dentate gyrus. (a) The total synapses number in punctum per μm^2 ($n = 3-6$ per group) was the addition of the number of excitatory synapses (Bassoon+PSD95 +) and inhibitory synapses (Bassoon+ Gephyrin+). There was a lower number of synapses at PND 8 in both PuM and OcM group compared to the sham group. * $p < 0.05$ between treatments. There were less synapses in PND 17 compared to PND 8. ## $p < 0.01$, ### $p < 0.001$ between ages. (b) Synapses balance was the ratio of number of excitatory synapses divided by the number of inhibitory synapses ($n = 4-6$ per group). At PND 8 the ratio was lower in both PuM and OcM groups compared with the sham group. * $p < 0.05$ between treatments. The ratio was lower in the PND 17 compared to the PND 8 for the sham and the PuM groups, respectively ## $p < 0.01$ and # $p < 0.05$ (c) Immunohistochemistry of sagittal brain slice at magnification $\times 60$ (scale bar = $20 \mu\text{m}$). Presynaptic bouton was immunolabeled with Bassoon (blue), inhibitory postsynaptic bouton was immunolabeled with gephyrin (red) and excitatory postsynaptic bouton synapses were immunolabelled with PSD-95 (green). PuM: general public whole body (wb) SAR for mothers; OcM: occupational whole body wbSAR for mothers. The violin plot provides a graphical representation of the distribution of individuals, where the width of the violin at any point reflects the data density. Quartiles are shown with continuous line and the median is indicated by a dotted line.

interaction $F_{1,27} = 0.01$ $p = 0.92$).

Data regarding Pu exposure effects on apoptosis were reported on Fig. 8c. The number of Apoptag positive cells was increased by the duration of exposure ($F_{1,26} = 3.86$ $p = 0.0001$) and by RF exposure ($F_{1,26} = 4.74$ $p = 0.04$) but was not modified by their interaction. The Bonferroni post-hoc t -test indicated that more NCSs entered in apoptosis in the 7-day sham-exposed vials compared to the 3-day sham-exposed vials ($p < 0.0001$) and that more NCSs entered in apoptosis in the 7-day RF-exposed vials compared to the 7-day sham-exposed vials ($p < 0.05$).

Data regarding Pu exposure effects on Ki-67 + cells were reported on Fig. 8d. The ratio of Ki-67 positive cells was increased with RF exposures ($F_{1,30} = 6.6$ $p = 0.015$) and exposure-duration ($F_{1,30} = 6.6$ $p < 0.0001$) but not by their interaction. After 7 days, the ratio of Ki-67 positive cells was higher in the RF-exposed compared to the sham-exposed ($p < 0.001$). It was also higher in the 7-day exposed (sham or Pu) compared to their respective 3-day vials (sham or Pu) ($p < 0.0001$ for both comparisons).

Data regarding Pu exposure effects on genotoxicity were reported on Fig. 8e. The ratio of γ -H2AX positive cells was increased with RF exposure ($F_{1,28} = 78.9$ $p < 0.0001$) and culture-duration ($F_{1,28} = 22.0$ $p < 0.0001$) as well as their interaction ($F_{1,28} = 8.4$ $p = 0.0071$). The ratio of γ -H2AX positive cells was increased in both 3-day RF-exposure and 7-day RF-exposure (+200 %) compared to their respective sham-exposed controls ($p < 0.001$ and $p < 0.0001$). The ratio of γ -H2AX positive cells was higher in the 7-day-RF-exposed cells compared to the

3-day-RF-exposed cells ($p < 0.0001$).

Altogether, the data indicate that RF exposure reduced apoptosis, and increased Ki-67 + cells and double strand breaks in DNA suggesting cell suffering from stress and the consecutive reactive entry into proliferation.

3.8. Three days after in vitro 7-day RF exposure NSCs maintained high Ki-67 + cells

Data regarding Pu exposure effects on cell growth were reported on Fig. 9a. Total cell number was reduced between the 3 and 7-day (sham or Pu) exposed cells ($F_{1,36} = 8.9$ $p = 0.0051$) but there was no effect of Pu.

Data regarding Pu exposure effects on Ki-67 + cells were reported on Fig. 9b. The ratio of Ki-67-positive cells was increased with RF exposure ($F_{1,24} = 7.7$ $p = 0.01$) and was significantly higher in the 7-day RF exposed compared with the 7-day sham exposed cells ($p < 0.05$). Thus, this effect observed right at the end of 7-day RF exposure was shown to maintain despite the absence of RF exposure for 3 additional days of cell culture.

Data regarding Pu exposure effects on oligodendrocyte progenitor cells (OPC) proliferation were reported on Fig. 9c. The ratio of Olig2-Ki-67 positive cells was increased with exposure-duration ($F_{1,23} = 6.8$ $p = 0.016$) and was significantly higher in the 7-day RF exposed compared with the 3-day RF exposed cells ($p < 0.05$). There was no PU effect.

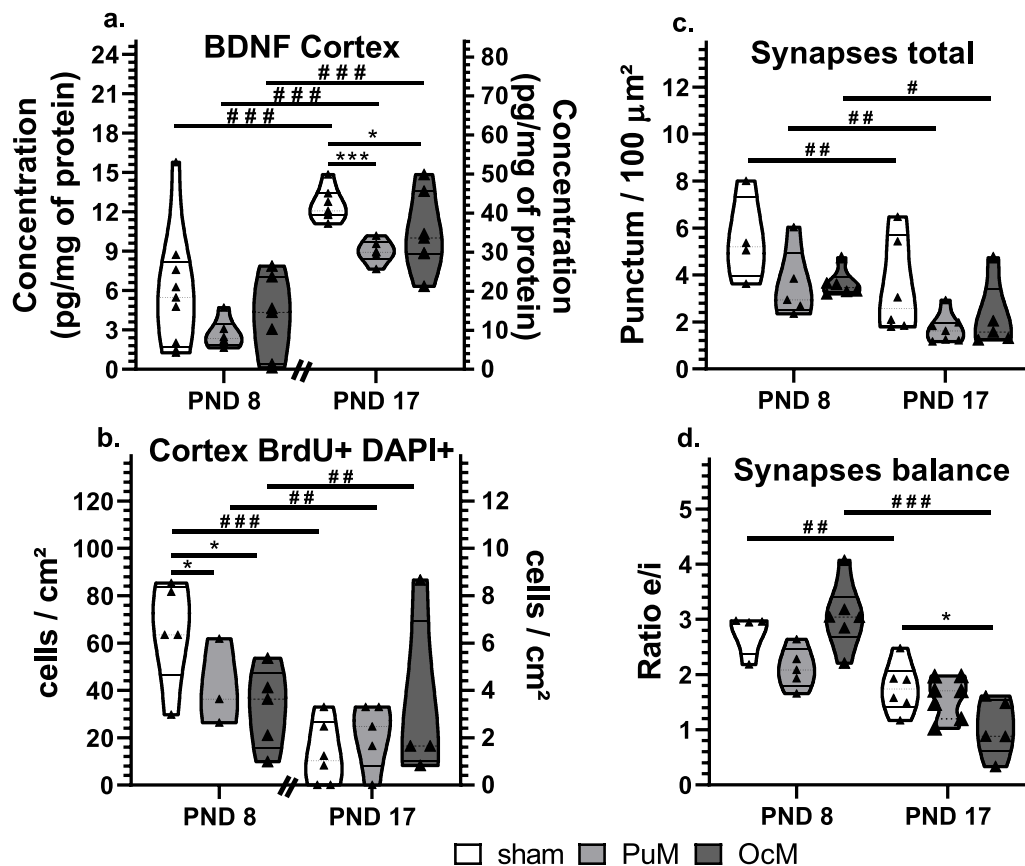


Fig. (6). Effect of RF-exposure from GD 8 to PND 8 or PND 17 on BrdU+ cells and synaptogenesis in the rat cortex. (a) BDNF concentration increased with age in all the groups and decreased at PND 17 in both PuM and OcM compared to sham group ($n = 6-9$). (b) Cells DAPI⁺ BrdU⁺ count per cm². There was a significant decrease in both PuM and OcM group at PND 8 compare to sham group. Proliferative cells were decrease significantly in all groups at PND 17 compared to PND 8 ($n = 3-6$). (c) Quantification of the total synapses number in punctum per µm² ($n = 4-7$): addition of excitatory synapses (Bassoon+PSD95+) and inhibitory synapses (Bassoon+ Gephyrin+). There were less synapses in PND 17 compared to PND 8. # $p < 0.05$, # # $p < 0.01$ between ages. (d) Synapses balance: ratio of number of excitatory synapses divided by inhibitory synapses ($n = 5-6$). Synapses ratio significantly decreased at PND17 in OcM group. Synapses ratios were lower at PND 17 compared to PND 8 only in OcM and sham groups. # # $p < 0.01$, # # # $p < 0.001$ between ages * $p < 0.05$, *** $p < 0.001$ between treatments. # $p < 0.05$, # # $p < 0.01$, # # # $p < 0.001$ between ages. PuM: general public whole body (wb) SAR for mothers; OcM: occupational whole body wbSAR for mothers. The violin plot provides a graphical representation of the distribution of individuals, where the width of the violin at any point reflects the data density. Quartiles are shown with continuous lines and the median is indicated by a dotted line.

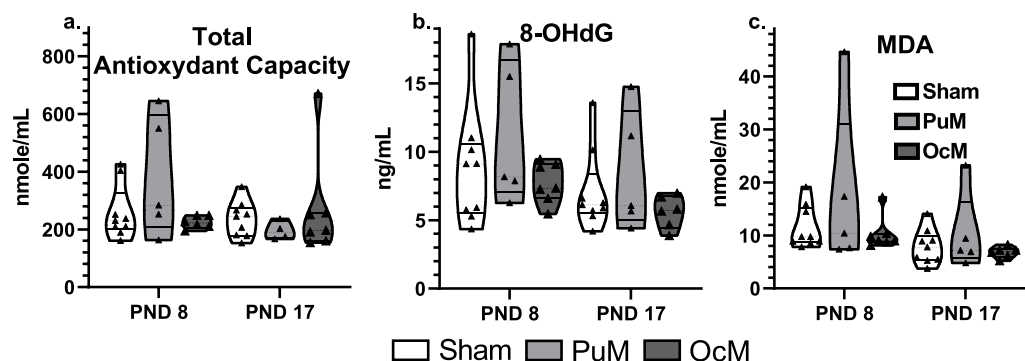


Fig. (7). RF-exposure from GD 8 to PND 8 or PND 17 effect on whole-brain oxidative stress markers of rats. (a) total antioxidant capacity. (b) 8-OHdG. (c) MDA ($n = 7-8$). 8-OHdG: 8-hydroxy-2'-deoxyguanosine; MDA: malondialdehyde; PuM: general public whole body (wb) SAR for mothers; OcM: occupational whole body wbSAR for mothers. The violin plot provides a graphical representation of the distribution of individuals, where the width of the violin at any point reflects the data density. Quartiles are shown with continuous lines and the median is indicated by a dotted line.

Altogether, the data indicate that Pu exposure increased Ki-67+ cells, a phenomenon which lasted after the end of Pu exposure, probably as a response to a stress situation.

3.9. Faster NSCs differentiation in vitro exposed to RF

The effect of Pu exposure on NCSs development was assessed with the ratio of the immature and differentiated cells (Fig. 10a and b). After a total of 10 days of culture NCSs, the most represented cells in the

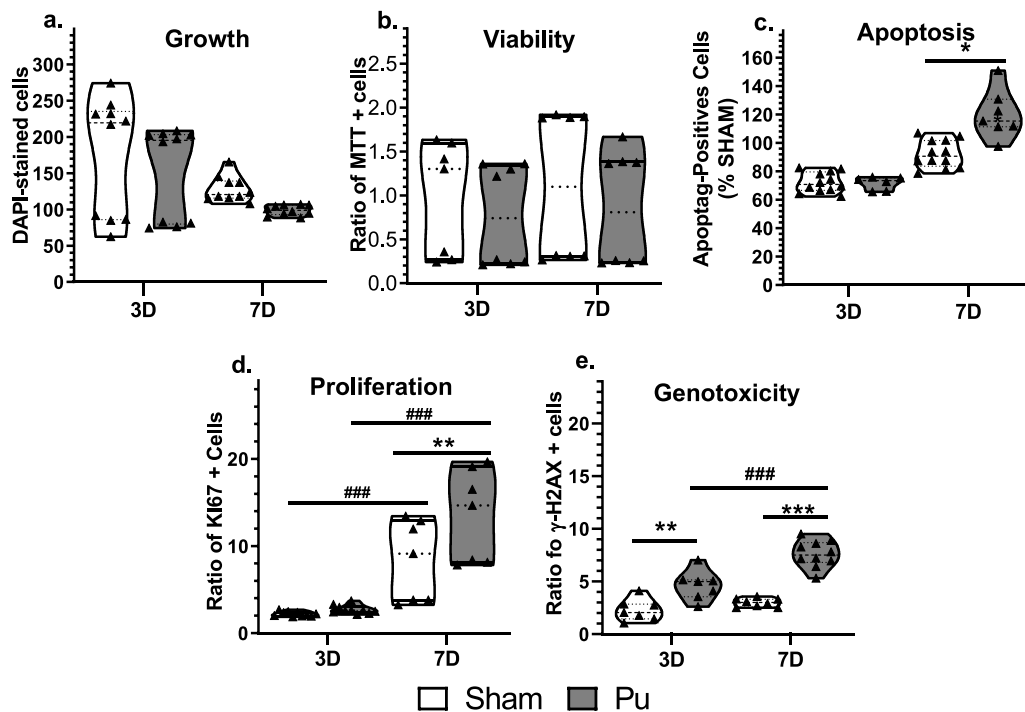


Fig. (8). Immediately at the end of RF exposure for either 3 or 7 days, total cell number (a), viability (b), apoptosis (c), Ki-67 + cells (d) and genotoxicity (e) from mouse were assessed. (a) Cell growth was assessed using the DAPI-stained cells. It was significantly reduced in the 7-day exposed cells compared with the 3-day. (b) Cell viability was assessed using the ratio of MTT positive cells. ### $p < 0.001$ versus the 3-day sham exposed cells; RF, duration of culture or their interaction had no effect on cell viability. (c) Apoptosis was assessed using the ratio of apoptag positive cells. * $p < 0.05$ versus the 7-day sham exposed cells; There was less apoptotic cells in the 7D-exposed group compared to the 7D-sham exposed group; * $p < 0.05$ versus the 7-day sham exposed cells. (d) Proliferation was assessed using the ratio of Ki-67 positive cells. ### $p < 0.001$ versus the respective 3-day-exposure-cell group (RF or sham). There was more Ki-67 + cells in the 7D-exposed group compared to the 7D-sham exposed group; *** $p < 0.001$ versus 7-day sham-exposed cells (e) Genotoxicity was assessed using the ratio of γ -H2AX positive cells to mark the double strand DNA breaks. ### $p < 0.001$ versus 3-day RF-exposed cells. There were more double DNA stand breaks in the RF exposed cells (for both 3 and 7 days) compared to their respective sham exposed cells; *** $p < 0.001$ versus 3-day sham-exposed cells; **** $p < 0.0001$ versus 7-day sham-exposed cells. (n = 9; an average of 150 cells analyzed per replicate). Pu: general public limit SAR exposure (0.08 W/kg). The violin plot provides a graphical representation of the distribution of individuals, where the width of the violin at any point reflects the data density. Quartiles are shown with continuous lines and the median is indicated by a dotted line.

decreasing order were the Nestin+ cells (C progenitor cells), the Nestin+ /GFAP+ (B1 cells) for the immature cells with the GFAP+ (astrocytes) and the Olig2 + (OPC) for the differentiated cells (Fig. 10c). Contingency test chi-square test did not indicate any difference in their repartition (Chi-square = 3.4, df = 9, $p = 0.94$). However, separate ANOVA for each cell type indicated significant cell type x Pu exposure interaction, cell type and Pu exposure effects (respectively, $F_{9,82} = 2.1$ $p = 0.037$, $F_{3,82} = 327.2$ $p < 0.0001$ and $F_{3,82} = 7.8$ $p = 0.0001$). The proportion of B1 cells was not dependent on exposure duration but reduced with RF exposure ($F_{1,19} = 8.9$ $p = 0.007$). The reduced ratio of B1 cells was significant in the 3D-RF-exposed cells compared to the 3D-sham-exposed (Bonferonni-corrected t -test: $p < 0.05$). The proportion of C cells was not dependent on exposure duration but was increased with Pu exposure ($F_{1,20} = 6.7$ $p = 0.017$).

The proportion of OPC increased with the duration of exposure (sham or Pu) ($F_{1,23} = 4.7$ $p = 0.04$) and with Pu exposure ($F_{1,23} = 13.2$ $p = 0.0014$). The ratio of OPC was significantly higher in the 7D-RF-exposed cells compared with the 7D-sham-exposed (Bonferonni-corrected t -test: $p < 0.01$).

The proportion of astrocytes was not dependent on exposure duration but was increased with Pu exposure ($F_{1,20} = 11.9$ $p = 0.0025$). The ratio of astrocytes was significantly higher in the 7D-RF-exposed cells compared to the 7D-sham-exposed (Bonferonni-corrected t -test: $p < 0.01$).

These results suggest that Pu exposure may accelerate NSCs differentiation.

4. Discussion

This study investigated the *in vivo* toxicity of 900 MHz RF-EMF at ICNIRP limits for public and occupational exposure. We assessed their effects on neural cell microenvironment and maturation in immature male rat pups through prenatal and postnatal exposures. Additionally, an *in vitro* toxicity assessment of NSCs at public exposure limits was conducted to corroborate *in vivo* findings.

Our global proteomic analysis revealed distinct protein expression profiles between the sham group and the exposed groups, as demonstrated by PCA analysis. At PND 0, ten differentially expressed proteins were identified, mainly associated with neuronal structuration, including synaptogenesis and proliferation. In the sham group, brain development was characterized by a reduction in BrdU+ cells, synapses, and excitatory/inhibitory balance between PND 8 and PND 17. RF-EMF exposure altered these neurodevelopmental processes. Specifically, reductions in BrdU+ cells in the cortex and synapses in the hippocampus were observed at PND 8 in both OcM and PuM groups. At later stages, BDNF levels decreased at PND 17 in both exposure conditions, together with synaptic imbalances in the cortex only at the higher wbSAR. *In vitro*, NSCs exhibited increased apoptosis, enhanced Ki-67 + cell proliferation, and double-strand DNA breaks following RF-EMF exposure. Notably, enhanced Ki-67 + cell proliferation persisted in PuM-exposed cells three days post-exposure. After a 10-day culture period, RF-EMF-exposed NSCs exhibited a lower ratio of B1 cells and an increased proportion of OPCs and astrocytes.

At PND0, even at the lowest SAR limit, the exposure to RF-EMF induces modification of protein expression. Decreased DRP1 and VPS45

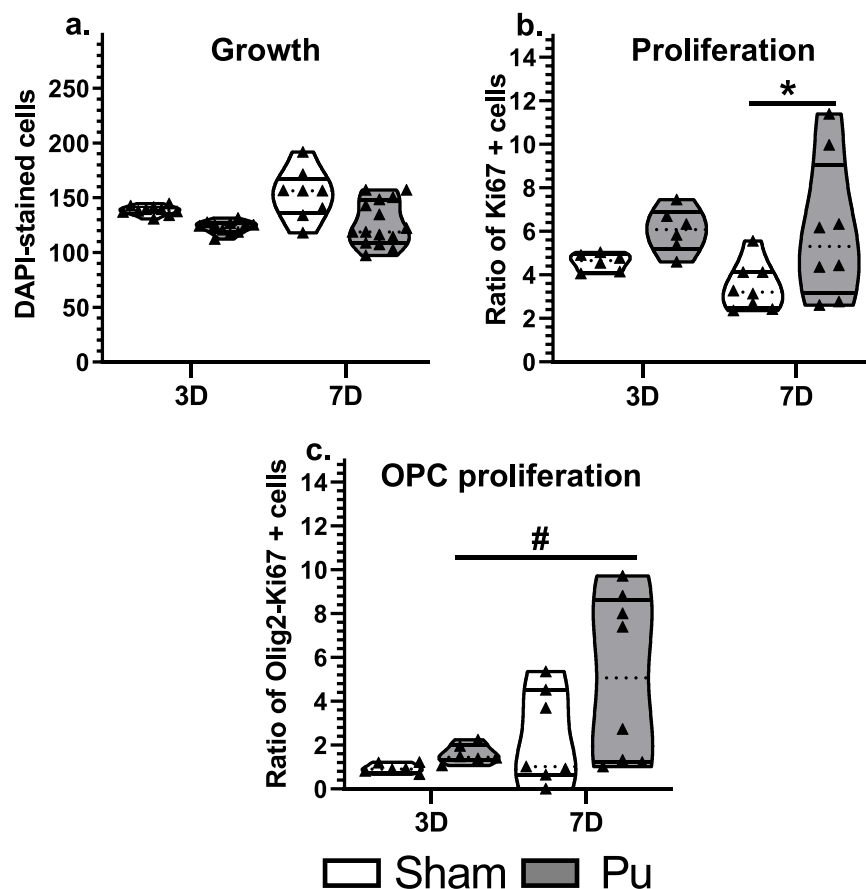


Fig. (9). Seven days after the end of the 3-day (RF or sham) exposure and 3 days after the 7-day (RF or sham) exposure, total cell number (a), Ki-67 + cells (b) and OPC Ki-67 + Olig2 + (c) from mouse were assessed. (a) Cell growth was assessed using the DAPI-stained cells. (b) Proliferation was assessed using the ratio of Ki-67 positive cells. There was more cell in Ki-67 + cells in the 7-day RF exposed cells compared with the 7-day sham exposed cells; * $p < 0.05$ higher versus the 7-day RF exposed 3-day cultured cells. (c) OPC proliferation was assessed using the ratio of cells co-expressing Olig2 and Ki-67. # $p < 0.05$ higher than the 3-day RF exposed cells. ($n = 9$; an average of 150 cells analyzed per replicate). Pu: general public limit SAR exposure (0.08 W/kg); OPC: oligodendrocyte progenitor cells. The violin plot provides a graphical representation of the distribution of individuals, where the width of the violin at any point reflects the data density. Quartiles are shown with continuous lines and the median is indicated by a dotted line.

have been observed concomitantly with higher Plexin A4 expression in OcM group in the hippocampus. DRP1 is part of the CRMP family involved in neuronal differentiation (Miyazaki et al., 2018) and axonal outgrowth with modulation of microtubule dynamics by interacting with tubulin and other cytoskeletal components (Lin et al., 2011; Yamashita and Goshima, 2012). DRP1 is a key factor in neuronal development and plasticity, influencing axonal guidance, growth cone collapse, and signal transduction pathways (Chua et al., 2021; Ravindran et al., 2022). Plexin A4 interacts with semaphorins, which are signaling molecules that mediate repulsive and attractive guidance cues. Plexin A4 is crucial for neural development, including axonal guidance, neuronal migration, and synaptic organization (Suto et al., 2007; Smolkin et al., 2018). The VPS45 is involved in protein recycling, degradation at the endosome and synaptic vesicle docking (Cowles et al., 1994; Vagnozzi and Praticò, 2019). Plexin A4 mediates signals from semaphorins, which are known to cause growth cone collapse and repulsion in neurons. DRP1 acts downstream of semaphorin signaling, contributing to cytoskeletal rearrangements necessary for these processes (Higurashi et al., 2012). The repulsive mechanism of semaphorin 3 A is mediated by the phosphorylation of CRMP2 (Uchida et al., 2005). Similar effects could be involved for DRP1 that might be phosphorylated or otherwise modified in response to Plexin A4 activation, altering its interaction with microtubules and affecting axon guidance and neuronal migration. This would result in the decreased total of synapses in the hippocampus observed at PND 8.

The decreased SOD (antioxidant enzyme) and zero beta-globin

(oxygen transport) in OcM group in the cortex, could indicate an involvement of oxidative stress mechanism (Chaves et al., 2013; Chidambaram et al., 2024). Concomitantly the increased of BAP18 in the cortex resulted in a cellular stress response. This protein is involved in chromatin remodeling and transcription regulation (Zhang et al., 2022). A delay in the cell cycle (G1 to S-phase transition) and increased apoptosis have been observed with a knockdown of BAP18 (Tang et al., 2021). The increase of BAP18, affecting the cell-cycle length, could indicate a compensatory response to the decreased BrdU+ cells that we observed in cortex region of the brain at PND 8, leading to decreased BDNF level at PND 17.

Few studies have performed quantitative proteomics following RF-EMF exposure. Wang et al. (2023) exposed adult rats for 6 weeks (6 min per day) at 9375 MHz or 2856 MHz at 10 mW/cm² and performed quantitative proteomic of hippocampal. The results indicate a decrease of SNARE-associated protein with increase charged multivesicular body protein 3, involved respectively in vesicle trafficking and synaptic vesicle recycling.

Confirming the hypothesis of an altered cellular proliferation by RF-EMF exposure at PND 0, we also observed a decreased BrdU+ cells in both PuM and OcM group at PND 8 in the cortical area. In this region, neurogenesis (new neuron generation) begins around GD 9.5 and last until PND 15 (Rice and Barone, 2000; Babikian et al., 2010). Similarly to our results, peripubertal rats (PND 35) exposed to 2115 MHz RF for 8 h continuously at 1.51 W/kg showed neuronal loss in dentate gyrus neurons but no effect on the CA3 and CA1 neurons of the hippocampus and

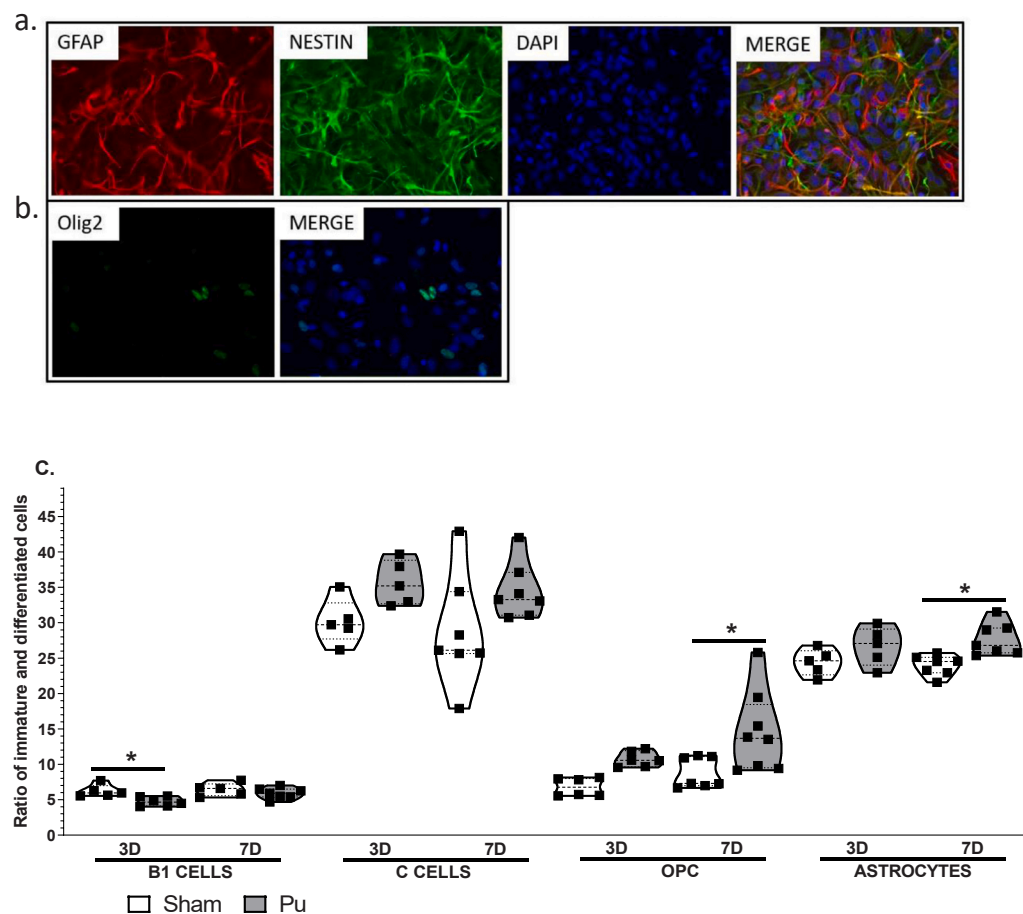


Fig. (10). Effect of 3 or 7-day RF-exposure on the ratio of immature and differentiated populations of SVZ precursor cells from mouse. (a) Immunocytochemistry of NSCs at magnification 40x (scale bar = 25 μ m). B1 cells were co-labelled for GFAP (red) and Nestin (green), a prototypic marker for undifferentiated NSCs. Astrocytes were identified as GFAP-positive cells (red). C cells were identified as Nestin-positive and GFAP-negative immunostained cells. (b) Immunocytochemistry of NSCs at magnification 40x (scale bar = 25 μ m). Oligodendrocyte progenitor cells were immunolabelled for Olig2 (green) (scale bar = 25 μ m). Arrows point to Olig2-positive cells. (c) Ratio of immature and differentiated cells after RF exposure. There was a lower ratio of B1 cells, higher ratio of C cells, OPC and astrocytes in the RF cells. * $p < 0.05$, the 3-day RF exposed cells contain a lower ratio of B1 cells compared to the 3-day sham exposed cells; The 7-day RF exposed cells contain a higher ratio of OPC compared to the 7-day sham exposed cells; The 7-day RF exposed cells contain a higher ratio of astrocytes compared to the 7-day sham exposed cells. (n = 9; an average of 150 cells analyzed per replicate). Pu: general public limit SAR exposure (0.08 W/kg); OPC: oligodendrocyte progenitor cells. The violin plot provides a graphical representation of the distribution of individuals, where the width of the violin at any point reflects the data density. Quartiles are shown with continuous lines and the median is indicated by a dotted line.

cerebral cortex (Singh et al., 2023). Exposing mice at 1800 MHz RF at 1.16 W/kg, 8 h daily for 3 days from PND 7 induced an increase in neural stem and progenitor cells, but reduced cell division and the total number of stem cells in the hippocampus (Xu et al., 2017).

Concomitantly with the results found *in vivo* on BrdU+ cells, we analyzed the effect of exposure at *in vitro* level by looking at the differentiation of NSC. We showed higher rate of Ki-67 + cells with reduced ratio of B1 cells (Ki-67 + cells / total cells) and increased ratio of C cells and of intermediate progenitor cells, the OPC and astrocytes with RF exposure. We also showed more apoptosis in the NSCs and in the astrocytes. The different results observed between Ki-67 + cells *in vitro* and BrdU+ cells *in vivo* can be explained by different factors. *In vitro* condition provides a controlled and isolated environment which can lead to direct effects of RF exposure on cell behavior. *In vitro* NSC differ from the NSC evolving *in vivo*, also due to their culture protocol. A study indicated that *in vitro* environment involve stress, leading to higher proliferation rate compared to *in vivo* (Urbán and Guillemot, 2014). Thus, the effects of RF-EMF exposures may be influenced by the *in vitro* environments which differs from the physiological environment. Parallely, the durations of exposure between the two models could leads to a stress response with increased cellular proliferation *in vitro* (3 or 7

days of RF exposure), whereas prolonged exposure *in vivo* lead to decreased proliferation (21 days of exposure at PND 8). Acute 900 MHz exposure of rats, resulted in the activation of p38/JNK-mediated MAPK pathway in rats testes (Er et al., 2022). This pathway is known to activate cellular proliferation in mammals (Zhang and Liu, 2002). This effect of acute exposure could also explain the differences between the two-exposure setups (*in vivo* and *in vitro*).

Regarding RF-EMF, divergent effects were reported on proliferation with decreased cell number in the cerebellum in adult rats exposed at 900 MHz (wbSAR: 0.016 W/kg) or no effects in embryonic-stem cell-derived neural progenitor culture exposed at 1710 MHz (SAR: 1.5 W/kg), (Nikolova et al., 2005; Sonmez et al., 2010). Also, many studies demonstrated no effect of RF-EMF on apoptosis of neural cells (Prochnow et al., 2011). For example, a SAR of 4 W/kg 1800-MHz RF-EMF exposure had no effect on the cell viability and apoptosis of embryonic NSCs. mRNA expression of apoptosis-related genes Bax and Bcl-2, indicated no significant effects after RF-EMF exposure (Chen et al., 2015). In contrast, a study suggested that 1950-MHz RF-EMF exposure may cause transcriptional changes in apoptosis related genes, such as Bax (Liu et al., 2012). The up-regulation of apoptosis-related genes has been observed in embryonic stem cell

derived neural progenitor cells *in vitro* (Joubert et al., 2007).

In vitro, we showed an increase in the number of DNA double breaks. Unlike ionizing radiation or ultraviolet light, the radiation emitted by RF is not sufficiently energetic, by several orders of magnitude, to directly damage macromolecules. However, studies suggest that non-thermal exposure of cells to RF may result in measurable genotoxic effects, despite varied and weak responses (Brusick et al., 1998; Ruediger, 2009). Induction of oxygen radicals or interference with DNA repair processes have been proposed as possible mechanism by which RF could cause DNA damage (Verschaeve et al., 2010). Effects were higher in amplitude and maintained after the end of exposure in the 7-day exposed groups while effects were weaker in amplitude and rarely maintained after the end of exposure in the 3-day exposed cells. Taken together, *in vitro* results may reveal cell suffering linked with DNA damage generating a compensatory mechanism that accelerate cell differentiation and/or proliferation but also apoptosis.

Total synapses and synapse balance showed significant decrease in all RF-exposed groups at PND 8 in the hippocampus. The synapse balance at PND 17 was also reduced in OcM group in the cortex area (mean ratio = 1.036). Though, increased neurons excitability was found in primary hippocampal neurons with 3000 MHz exposure (SAR < 1 W/kg) for 60 min *in vitro* (Echchgadda et al., 2022). Increased excitability has also been observed *ex vivo* with slices of hippocampus exposed at 700 MHz (SAR: 0.0016 W/kg – 0.0044 W/kg) during 5 or 15 min (Tattersall et al., 2001). The decreased synapses balance observed *in vivo* could be the response of the organism to this increased excitability due to RF-EMF exposure. This increased inhibition *in vivo* has been observed previously with RF-EMF exposure of juvenile rats to 1800 MHz, with SAR value of 0.843 W/kg, 1 h daily for 1 month, inducing significant decreases in glutamate and glutamine levels (excitatory amino acids) in hippocampus and glutamine level also decreased significantly after 4 months of exposure (Ahmed et al., 2018). Noor et al. (2011) investigated the effect of 1-hour daily exposure of young rats to 900 MHz with wbSAR value of 1.165 W/kg. A significant glycine increase in the midbrain was observed after 1 month, followed by a significant increase in GABA after 4 months. *In vivo* exposure of adult rats to 5800 MHz for 2 or 4 h at wbSAR of 1.15 W/kg showed no effect on PSD95 levels in the hippocampus region (Rui et al., 2022). Reduced NMDAR1 and AMPAR1 (mediators of excitatory neurotransmission) levels in the hippocampus were observed when mice were exposed 5 h per day for 4 weeks (from P1 to P28) at 1850 MHz RF-EMF at 4 W/kg wbSAR (Kim et al., 2021). The difference of effects found *in vivo* and *in vitro* seems to indicate that the fully developed organism may compensate to avoid the increased excitability that has been observed *in vivo*.

In a study realized by Majdi et al., (2007), (2009), an association between age-related cognitive impairment and postsynaptic imbalance toward inhibition in the cortex of adult rats have been observed. These results have also been shown in other studies (Luebke et al., 2004; Wong et al., 2006). In human prefrontal cortex, aging was shown to induce decreased BDNF level inducing inhibitory and excitatory synaptic alteration (Oh et al., 2016). In the cortical area, we showed a significant reduction in BDNF level only at PND 17 for both PuM and OcM groups. The expression of BDNF during neonatal period is dependent of the brain region. In the cortex, the expression has been recorded from PND 4 in mice (Baquet et al., 2004). In the cortex area, BDNF levels were found at 10 pg/mg of protein in adult rats (Mannari et al., 2008) and 0.06 pg/mg of protein in adult rat (Gelfo et al., 2011). At different frequency (2650 MHz) for 28 days at 2.06 W/kg for 4 h per day, adult male mice showed reduced expression of BDNF protein in the hippocampus (Zheng et al., 2023). Adult male mice also showed decreased BDNF in the auditory brainstem nuclei after 835 MHz exposure with SAR of 1.6 W/kg, 8 h per day for 3 months (Maskey and Kim, 2014). In our study, BDNF level were significantly increased between PND 8 and PND 17 in all groups. BDNF level in the cortex reach a peak between PND 10 and PND 30 (Esveld et al., 2023). Our results could indicate a lower peak of expression at PND 17 for RF-exposed groups leading to exacerbate the

decrease of synaptic balance in the cortex between PND 8 and PND 17.

The pups analysed in the present study are the same as those reported in our previous publication on physical development, which showed lower body weight from PND 6 to PND 43 in the OcM group (Bodin et al., 2024). In the present study, a significant reduction in BDNF levels was observed at PND 17 in both the PuM and OcM groups. Similarly, Kim et al. (2021) demonstrated that mice exposed to 1850 MHz radio-frequency radiation from PND 1 to PND 28, for 5 h per day at a specific absorption rate (SAR) of 4 W/kg exhibited reduced BDNF levels in the hippocampus. Conversely, exposure to a Wi-Fi signal (2450 MHz) at an electric field strength of 21 V/m for 24 h per day, from gestational day (GD) 0 for a duration of 9 weeks, resulted in weight gain in male pups at PND 28, PND 35, and PND 42. This weight gain coincided with an increase in hippocampal BDNF levels at PND 43 (Wu et al., 2023). Similarly, DastAmooz et al., (2023) exposed pregnant rats to 2400 MHz Wi-Fi radiation for 6 h per day from GD 0 until delivery, with a whole-body SAR ranging between 0.15 W/kg and 0.31 W/kg. Their findings indicated a significant reduction in pup weight at birth; however, no significant differences were observed at PND 21 or PND 56. Additionally, hippocampal BDNF levels were significantly reduced at PND 56. A comparable effect on hippocampal BDNF was reported in adult rats exposed to 900 MHz electromagnetic fields at an electric field strength of 6 V/m for 1 h per day over 15 days (Ustunova et al., 2022). Notably, in the studies by Wu et al. (2023) and DastAmooz et al., (2023), changes in hippocampal BDNF levels (both increases and decreases) were correlated with corresponding variations in body weight.

5. Conclusion

The present data suggest that during prenatal development, continuous wave RF-EMF exposures at regulatory thresholds decrease cellular proliferation, alter differentiation, and decrease synaptogenesis in the immature brain of rodents. PND 8 and 17 appear to be critical windows of age for the expression of impairments of neurodevelopment. In the specific endpoints of the present protocol, the 9 days longer duration exposure reached at PND 17 compared with PND 8 did not reinforce or even maintain the cellular proliferation or synaptic impairment at PND 8 despite the higher amount of cumulative absorbed energy. These data support the hypothesis of a vulnerability of developing organisms towards RF-EMF exposures and to maintain caution regarding RF-EMF exposures of pregnant women and young children during telecommunication use.

CRedit authorship contribution statement

Sarah Méresse: Writing – review & editing, Methodology, Investigation. **Paulo Marcelo:** Writing – review & editing, Methodology, Investigation. **Céline Montécot-Dubourg:** Writing – review & editing, Methodology, Investigation. **Lucas Godin:** Writing – review & editing, Methodology, Investigation, Conceptualization. **Raphaël Bodin:** Writing – review & editing, Writing – original draft, Methodology, Investigation, Formal analysis, Conceptualization. **Anne-Sophie Villégier:** Writing – review & editing, Supervision, Methodology, Investigation, Funding acquisition, Conceptualization. **Stéphane Mortaud:** Writing – review & editing, Supervision, Methodology, Investigation, Funding acquisition, Conceptualization. **Justyne Feat-Vetel:** Writing – review & editing, Methodology, Investigation, Conceptualization. **Vanessa Larrigaldie:** Writing – review & editing, Methodology, Investigation. **Anthony Lecomte:** Methodology, Investigation. **Camille Mougin:** Writing – review & editing, Methodology, Investigation, Conceptualization.

Ethical approval

Protocols were validated by the Regional Ethical Committee (CRE-MEAP N. 96) and the French Ministry of Research (APAFIS#19003, 26/08/2019; Bodin et al., 2024) and complied with the decree on vertebrate animal experiments (French State Council, 1987). For mice experimentation, all experimentation and animal care respected the European Communities Council directive (2010/63/EU) and the French Minister under APAFIS#21860.

Consent to Participate

This is not applicable.

Consent to Publish

All authors approve to publish the manuscript.

Funding

Funder: French Ministry of Ecology Program 190.

Declaration of Competing Interest

The authors declare that they have no competing interests.

Acknowledgements

Not applicable

Data availability

Data will be made available on request.

References

- Abrous, D.N., Koehl, M., Le Moal, M., 2005. Adult neurogenesis: from precursors to network and physiology (Apr). *Physiol. Rev.* 85 (2), 523–569. <https://doi.org/10.1152/physrev.00055.2003>.
- Ackermann, F., Waites, C.L., Garner, C.C., 2015. Presynaptic active zones in invertebrates and vertebrates (Aug). *EMBO Rep.* 16 (8), 923–938. <https://doi.org/10.15252/embr.201540434>.
- Ahmed, N.A., Radwan, N.M., Aboul Ezz, H.S., Khadrawy, Y.A., Salama, N.A., 2018. The chronic effect of pulsed 1800 MHz electromagnetic radiation on amino acid neurotransmitters in three different areas of juvenile and young adult rat brain (Dec). *Toxicol. Ind. Health* 34 (12), 860–872. <https://doi.org/10.1177/0748233718798975>.
- Albore-Garcia, D., McGlothlin, J.L., Guilarte, T.R., 2021. Early-life lead exposure and neurodevelopmental disorders (Jun). *Curr. Opin. Toxicol.* 26, 22–27. <https://doi.org/10.1016/j.cotox.2021.03.007>.
- Alvarez-Buylla, A., Lim, D.A., 2004. For the long run: maintaining germinal niches in the adult brain. *Mar 4 Neuron* 41 (5), 683–686. [https://doi.org/10.1016/S0896-6273\(04\)00111-4](https://doi.org/10.1016/S0896-6273(04)00111-4).
- Antoine, M.W., Langberg, T., Schnepel, P., Feldman, D.E., 2019. Increased Excitation-Inhibition ratio stabilizes synapse and circuit excitability in four autism mouse models. *Feb 20 Neuron* 101 (4), 648–661.e4. <https://doi.org/10.1016/j.neuron.2018.12.026>.
- Babikian, T., Prins, M.L., Cai, Y., Barkhoudarian, G., Hartonian, I., Hovda, D.A., Giza, C. C., 2010. Molecular and physiological responses to juvenile traumatic brain injury: focus on growth and metabolism. *Dev. Neurosci.* 32 (5–6), 431–441. <https://doi.org/10.1159/000320667>.
- Baquet, Z.C., Gorski, J.A., Jones, K.R., 2004. Early striatal dendrite deficits followed by neuron loss with advanced age in the absence of anterograde cortical brain-derived neurotrophic factor. *Apr 28 J. Neurosci.* 24 (17), 4250–4258. <https://doi.org/10.1523/JNEUROSCI.3920-03.2004>.
- Bhatt, C.R., Thielens, A., Billah, B., Redmayne, M., Abramson, M.J., Sim, M.R., Vermeulen, R., Martens, L., Joseph, W., Benke, G., 2016. Assessment of personal exposure from radiofrequency-electromagnetic fields in Australia and Belgium using on-body calibrated exposimeters (Nov). *Environ. Res* 151, 547–563. <https://doi.org/10.1016/j.envres.2016.08.022>.
- Bodin, Raphaël, Robidel, Franck, Rodrigues, Stéphanie, Lecomte, Anthony, Villégier, Anne-Sophie, 2024. "Delayed growth in immature Male rats exposed to 900 MHz radiofrequency". *Appl. Sci.* 14 (16), 6978. <https://doi.org/10.3390/app14166978>.
- Borchert, Astrid, Wang, Chi Chiu, Ufer, Christoph, Schiebel, Heike, Savaskan, Nicolai E., Kuhn, Hartmut, 2006. The role of phospholipid hydroperoxide glutathione peroxidase isoforms in murine embryogenesis*, 14 July J. Biol. Chem. 281 (28), 19655–19664. <https://doi.org/10.1074/jbc.M601195200>.
- Bozzi, Y., Provenzano, G., Casarosa, S., 2018. Neurobiological bases of autism-epilepsy comorbidity: a focus on excitation/inhibition imbalance (Mar). *Eur. J. Neurosci.* 47 (6), 534–548. <https://doi.org/10.1111/ejn.13595>.
- Briones, T.L., Woods, J., 2013. Chronic binge-like alcohol consumption in adolescence causes depression-like symptoms possibly mediated by the effects of BDNF on neurogenesis. *Dec 19 Neuroscience* 254, 324–334. <https://doi.org/10.1016/j.neuroscience.2013.09.031>.
- Brusick, D., Albertini, R., McRee, D., Peterson, D., Williams, G., Hanawalt, P., Preston, J., 1998. Genotoxicity of radiofrequency radiation. Dna/genetox expert panel. *Environ. Mol. Mutagen* 32 (1), 1–16. [https://doi.org/10.1002/\(sici\)1098-2280\(1998\)32:1<1:aid-em1>3.0.co;2-q](https://doi.org/10.1002/(sici)1098-2280(1998)32:1<1:aid-em1>3.0.co;2-q).
- Capstick, M., Kuster, N., Kuehn, S., Berdinas-Torres, V., Gong, Y., Wilson, P., Ladbury, J., Koepke, G., McCormick, D.L., Gauger, J., Melnick, R.L., 2017. A radio frequency radiation exposure system for rodents based on reverberation chambers (Aug). *IEEE Trans. Electro Compat.* 59 (4), 1041–1052. <https://doi.org/10.1109/TEMC.2017.2649885>.
- Çelik, Ö., Kahya, M.C., Nazıroğlu, M., 2016. Oxidative stress of brain and liver is increased by Wi-Fi (2.45GHz) exposure of rats during pregnancy and the development of newborns (Sep). *J. Chem. Neuroanat.* 75 (Pt B), 134–139. <https://doi.org/10.1016/j.jchemneu.2015.10.005>.
- Chaves, D.F., Carvalho, P.C., Lima, D.B., Nicastro, H., Lorenzetti, F.M., Siqueira-Filho, M., Hirabara, S.M., Alves, P.H., Moresco, J.J., Yates, J.R., 3rd, Lancha Jr., A.H., 2013. Comparative proteomic analysis of the aging soleus and extensor digitorum longus rat muscles using TMT labeling and mass spectrometry. *Oct 4 J. Proteome Res* 12 (10), 4532–4546. <https://doi.org/10.1021/pr400644x>.
- Chen, C., Ma, Q., Liu, C., Deng, P., Zhu, G., Zhang, L., He, M., Lu, Y., Duan, W., Pei, L., Li, M., Yu, Z., Zhou, Z., 2015. Exposure to 1800 MHz radiofrequency radiation impairs neurite outgrowth of embryonic neural stem cells. *Sci. Rep.* 4, 5103. <https://doi.org/10.1038/srep05103>.
- Chidambaram, S.B., Anand, N., Varma, S.R., Ramamurthy, S., Vichitra, C., Sharma, A., Mahalakshmi, A.M., Essa, M.M., 2024. Superoxide dismutase and neurological disorders. *Jan 23 IBRO Neurosci. Rep.* 16, 373–394. <https://doi.org/10.1016/j.ibneur.2023.11.007>.
- Chua, J.Y., Ng, S.J., Yagensky, O., Wanker, E.E., Chua, J.J.E., 2021. FEZ1 forms complexes with CRMP1 and DCC to regulate axon and dendrite development. *Apr 16 eNeuro* 8 (2), ENEURO.0193-20.2021. <https://doi.org/10.1523/ENEURO.0193-20.2021>.
- Cowles, C.R., Emr, S.D., Horazdovsky, B.F., 1994. Mutations in the VPS45 gene, a SEC1 homologue, result in vacuolar protein sorting defects and accumulation of membrane vesicles (December). *J. Cell Sci.* 110 (12), 3449–3459. <https://doi.org/10.1242/jcs.107.12.3449>.
- DastAmooz, S., Broujeni, S.T., Sarhian, N., 2023. A primary study on rat fetal development and brain-derived neurotrophic factor levels under the control of electromagnetic fields. *Apr 19 J. Public Health Afr.* 14 (6), 2347. <https://doi.org/10.4081/jphia.2023.2347>.
- Del Vecchio, G., Giuliani, A., Fernandez, M., Mesirca, P., Bersani, F., Pinto, R., Ardoino, L., Lovisolo, G.A., Giardino, L., Calzà, L., 2009. Continuous exposure to 900MHz GSM-modulated EMF alters morphological maturation of neural cells. *May 22 Neurosci. Lett.* 455 (3), 173–177. <https://doi.org/10.1016/j.neulet.2009.03.061>.
- Delgheyr, Nathalie, Meunier, Alice, Faucourt, Marion, Bosch, Grau, Montserrat, Strehl, Laetitia, Janke, Carsten, Spassky, Nathalie, 2015. Chapter 2 - ependymal cell differentiation, from monolayer to multiciliated cells. In: Basto, Renata, Wallace, Marshall, F. (Eds.), *In Methods in Cell Biology*, edited by, 127. Academic Press, Methods in Cilia & Flagella, pp. 19–35. <https://doi.org/10.1016/bs.mcb.2015.01.004>.
- Dos Reis, R., Kornobis, E., Pereira, A., Tores, F., Carrasco, J., Gautier, C., Jahannault-Talignani, C., Nitschké, P., Muchardt, C., Schlosser, A., Maric, H.M., Ango, F., Allemand, E., 2022. Complex regulation of gephyrin splicing is a determinant of inhibitory postsynaptic diversity. *Jun 18 Nat. Commun.* 13 (1), 3507. <https://doi.org/10.1038/s41467-022-31264-w>.
- Echchgadda, I., Cantu, J.C., Tolstykh, G.P., Butterworth, J.W., Payne, J.A., Ibey, B.L., 2022. Changes in the excitability of primary hippocampal neurons following exposure to 3.0 GHz radiofrequency electromagnetic fields. *Mar 3 Sci. Rep.* 12 (1), 3506. <https://doi.org/10.1038/s41598-022-06914-0>.
- Eghlidospour, M., Ghanbari, A., Mortazavi, S.M.J., Azari, H., 2017. Effects of radiofrequency exposure emitted from a GSM mobile phone on proliferation, differentiation, and apoptosis of neural stem cells (Jun). *Anat. Cell Biol.* 50 (2), 115–123. <https://doi.org/10.5115/acb.2017.50.2.115>.
- Er, H., Tas, G.G., Soygun, B., Ozen, S., Sati, L., 2022. Acute and chronic exposure to 900 MHz radio frequency radiation activates p38/JNK-mediated MAPK pathway in rat testis (May). *Reprod. Sci.* 29 (5), 1471–1485. <https://doi.org/10.1007/s43032-022-00844-y>.
- Esvald, E.E., Tuvikene, J., Kiir, C.S., Avarlaid, A., Tamberg, L., Sirp, A., Shubina, A., Cabrera-Cabrera, F., Pihlak, A., Koppel, I., Palm, K., Timmusk, T., 2023. Revisiting the expression of BDNF and its receptors in mammalian development. *Jun 22 Front Mol. Neurosci.* 16, 1182499. <https://doi.org/10.3389/fnmol.2023.1182499>.
- Fatima, M., Srivastav, S., Ahmad, M.H., Mondal, A.C., 2019. Effects of chronic unpredictable mild stress induced prenatal stress on neurodevelopment of neonates: role of GSK-3β. *Feb 4 Sci. Rep.* 9 (1), 1305. <https://doi.org/10.1038/s41598-018-38085-2>.
- Gallucci, S., Focchi, S., Bonato, M., Chiaramello, E., Tognola, G., Parazzini, M., 2022. Exposure assessment to radiofrequency electromagnetic fields in occupational

- military scenarios: a review. Jan 14 Int J. Environ. Res Public Health 19 (2), 920. <https://doi.org/10.3390/ijerph19020920>.
- Gelfo, F., Cuttuli, D., Foti, F., Laricchiuta, D., De Bartolo, P., Caltagirone, C., Petrosini, L., Angelucci, F., 2011. Enriched environment improves motor function and increases neurotrophins in hemispheric lesions in rats (Mar-Apr). *Neurorehabil Neural Repair* 25 (3), 243–252. <https://doi.org/10.1177/1545968310380926>.
- Grandjean, P., Landrigan, P.J., 2014. Neurobehavioural effects of developmental toxicity (Mar). *Lancet Neurol.* 13 (3), 330–338. [https://doi.org/10.1016/S1474-4422\(13\)70278-3](https://doi.org/10.1016/S1474-4422(13)70278-3). Epub 2014 Feb 17.
- Groeneweg, F.L., Trattinig, C., Kuhse, J., Nawrotzki, R.A., Kirsch, J., 2018. Gephyrin: a key regulatory protein of inhibitory synapses and beyond (Nov). *Histochem Cell Biol.* 150 (5), 489–508. <https://doi.org/10.1007/s00418-018-1725-2>.
- Haubensack, W., Attardo, A., Denk, W., Huttner, W.B., 2004. Neurons arise in the basal neuroepithelium of the early mammalian telencephalon: a major site of neurogenesis. *Mar 2 Proc. Natl. Acad. Sci. USA* 101 (9), 3196–3201. <https://doi.org/10.1073/pnas.0308600100>.
- Hayes, N.L., Nowakowski, R.S., 2002. Dynamics of cell proliferation in the adult dentate gyrus of two inbred strains of mice. *Mar 31 Brain Res Dev. Brain Res* 134 (1–2), 77–85. [https://doi.org/10.1016/S0165-3806\(01\)00324-8](https://doi.org/10.1016/S0165-3806(01)00324-8).
- Higurashi, M., Iketani, M., Takei, K., Yamashita, N., Aoki, R., Kawahara, N., Goshima, Y., 2012. Localized role of CRMP1 and CRMP2 in neurite outgrowth and growth cone steering (Dec). *Dev. Neurobiol.* 72 (12), 1528–1540. <https://doi.org/10.1002/dneu.22017>.
- Hoshino, K., Matsuzawa, T., Murakami, U., 1973. Characteristics of the cell cycle of matrix cells in the mouse embryo during histogenesis of telencephalon. *Mar 15 Exp. Cell Res* 77 (1), 89–94. [https://doi.org/10.1016/0014-4827\(73\)90556-9](https://doi.org/10.1016/0014-4827(73)90556-9).
- Hussein, S., El-Saba, A.A., Galal, M.K., 2016. Biochemical and histological studies on adverse effects of mobile phone radiation on rat's brain (Dec). *J. Chem. Neuroanat.* 78, 10–19. <https://doi.org/10.1016/j.jchemneu.2016.07.009>.
- Joubert, V., Leveque, P., Cueille, M., Bourthoumieu, S., Yardin, C., 2007. No apoptosis is induced in rat cortical neurons exposed to GSM phone fields. *Bioelectromagnetics* 28, 115–121. <https://doi.org/10.1002/bem.20274>.
- Keith, D., El-Husseini, A., 2008. Excitation control: balancing PSD-95 function at the synapse. *Mar 28 Front Mol. Neurosci.* 1, 4. <https://doi.org/10.3389/neuro.02.004.2008>.
- Kim, E., Sheng, M., 2004. PDZ domain proteins of synapses (Oct). *Nat. Rev. Neurosci.* 5 (10), 771–781. <https://doi.org/10.1038/nrn1517>.
- Kim, J.H., Kim, H.J., Yu, D.H., Kwon, H.S., Huh, Y.H., Kim, H.R., 2017. Changes in numbers and size of synaptic vesicles of cortical neurons induced by exposure to 835 MHz radiofrequency-electromagnetic field. *Oct 18 PLoS One* 12 (10), e0186416. <https://doi.org/10.1371/journal.pone.0186416>.
- Kim, J.H., Lee, C.H., Kim, H.G., Kim, H.R., 2019. Decreased dopamine in striatum and difficult locomotor recovery from MPTP insult after exposure to radiofrequency electromagnetic fields. *Feb 4 Sci. Rep.* 9 (1), 1201. <https://doi.org/10.1038/s41598-018-37874-z>.
- Kim, J.H., Chung, K.H., Hwang, Y.R., Park, H.R., Kim, H.J., Kim, H.G., Kim, H.R., 2021. Exposure to RF-EMF alters postsynaptic structure and hinders neurite outgrowth in developing hippocampal neurons of early postnatal mice. *May 19 Int J. Mol. Sci.* 22 (10), 5340. <https://doi.org/10.3390/ijms22105340>.
- Knuesel, I., Zuellig, R.A., Schaub, M.C., Fritschy, J.M., 2001. Alterations in dystrophin and utrophin expression parallel the reorganization of GABAergic synapses in a mouse model of temporal lobe epilepsy (Mar). *Eur. J. Neurosci.* 13 (6), 1113–1124. <https://doi.org/10.1046/j.0953-816x.2001.01476.x>.
- Laval, L., Leveque, P., Jecko, B., 2000. A new in vitro exposure device for the mobile frequency of 900 MHz (May). *Bioelectromagnetics* 21 (4), 255–263. [https://doi.org/10.1002/\(sici\)1521-186x\(200005\)21:4<255::aid-bem2>3.0.co;2-4](https://doi.org/10.1002/(sici)1521-186x(200005)21:4<255::aid-bem2>3.0.co;2-4).
- Lin, P.C., Chan, P.M., Hall, C., Manser, E., 2011. Collapsin response mediator proteins (CRMPs) are a new class of microtubule-associated protein (MAP) that selectively interacts with assembled microtubules via a taxol-sensitive binding interaction. *Dec 2 J. Biol. Chem.* 286 (48), 41466–41478. <https://doi.org/10.1074/jbc.M111.283580>.
- Liu, Yu-xiao, Tai, J., Li, G., Zhang, Z., Xue, J., Liu, H., Zhu, H., Cheng, J., Liu, Yuan-ling, Li, A., Zhang, Y., 2012. Exposure to 1950-MHz TD-SCDMA electromagnetic fields affects the apoptosis of astrocytes via Caspase-3-Dependent pathway. *PLoS ONE* 7, e42332. <https://doi.org/10.1371/journal.pone.0042332>.
- Londino Tobon, A., Diaz Stransky, A., Ross, D.A., Stevens, H.E., 2016. Effects of maternal prenatal stress: mechanisms, implications, and novel therapeutic interventions. *Dec 1 Biol. Psychiatry* 80 (11), e85–e87. <https://doi.org/10.1016/j.biopsych.2016.09.011>.
- Luebke, J.I., Chang, Y.M., Moore, T.L., Rosene, D.L., 2004. Normal aging results in decreased synaptic excitation and increased synaptic inhibition of layer 2/3 pyramidal cells in the monkey prefrontal cortex. *Neuroscience* 125 (1), 277–288. <https://doi.org/10.1016/j.neuroscience.2004.01.035>.
- Majdi, M., Ribeiro-da-Silva, A., Cuello, A.C., 2007. Cognitive impairment and transmitter-specific pre- and postsynaptic changes in the rat cerebral cortex during ageing (Dec). *Eur. J. Neurosci.* 26 (12), 3583–3596. <https://doi.org/10.1111/j.1460-9568.2007.05966.x>.
- Majdi, M., Ribeiro-da-Silva, A., Cuello, A.C., 2009. Variations in excitatory and inhibitory postsynaptic protein content in rat cerebral cortex with respect to aging and cognitive status. *Mar 17 Neuroscience* 159 (2), 896–907. <https://doi.org/10.1016/j.neuroscience.2008.11.034>.
- Mannari, C., Origlia, N., Scatena, A., Del Debbio, A., Catena, M., Dell'agnello, G., Barraco, A., Giovannini, L., Dell'osso, L., Domenici, L., Piccinini, A., 2008. BDNF level in the rat prefrontal cortex increases following chronic but not acute treatment with duloxetine, a dual acting inhibitor of noradrenaline and serotonin re-uptake (May). *Cell Mol. Neurobiol.* 28 (3), 457–468. <https://doi.org/10.1007/s10571-007-9254-x>.
- Maskey, D., Kim, M.J., 2014. Immunohistochemical localization of brain-derived neurotrophic factor and glial cell line-derived neurotrophic factor in the superior olivary complex of mice after radiofrequency exposure. *Apr 3 Neurosci. Lett.* 564, 78–82. <https://doi.org/10.1016/j.neulet.2014.02.013>.
- Maskey, D., Kim, M., Aryal, B., Pradhan, J., Choi, I.Y., Park, K.S., Son, T., Hong, S.Y., Kim, S.B., Kim, H.G., Kim, M.J., 2010. Effect of 835 MHz radiofrequency radiation exposure on calcium binding proteins in the hippocampus of the mouse brain. *Feb 8 Brain Res* 1313, 232–241. <https://doi.org/10.1016/j.brainres.2009.11.079>. Epub 2009 Dec 5.
- Menn, B., Garcia-Verdugo, J.M., Yaschine, C., Gonzalez-Perez, O., Rowitch, D., Alvarez-Buylla, A., 2006. Origin of oligodendrocytes in the subventricular zone of the adult brain. *Jul 26 J. Neurosci.* 26 (30), 7907–7918. <https://doi.org/10.1523/JNEUROSCI.1299-06.2006>.
- Miyazaki, T., T. Baba, T., Mori, M., Komori, T., 2018. Collapsin response mediator protein 1, a novel marker protein for differentiated odontoblasts. *Dec 20 Acta Histochem Cytochem* 51 (6), 185–190. <https://doi.org/10.1267/ahc.18030>.
- Monday, H.R., Younts, T.J., Castillo, P.E., 2018. Long-Term plasticity of neurotransmitter release: emerging mechanisms and contributions to brain function and disease. *Jul 8 Annu Rev. Neurosci.* 41, 299–322. <https://doi.org/10.1146/annurev-neuro-080317-062155>.
- Narayanan, S.N., Mohapatra, N., John, P., K N, Kumar, R.S., Nayak, S.B., Bhat, P.G., 2018. Radiofrequency electromagnetic radiation exposure effects on amygdala morphology, place preference behavior and brain caspase-3 activity in rats (Mar). *Environ. Toxicol. Pharm.* 58, 220–229. <https://doi.org/10.1016/j.etap.2018.01.009>.
- Nikolova, T., Czyz, J., Rolletschek, A., Blyszczuk, P., Fuchs, J., Jovtchev, G., Schuldner, J., Kuster, N., Wobus, N.A., 2005. Electromagnetic fields affect transcript levels of apoptosis-related genes in embryonic stem cell-derived neural progenitor cells. *FASEB J.* 19, 1686–1688. <https://doi.org/10.1096/fj.04-3549fj>.
- Nishimura, Y., Kanda, Y., Sone, H., Aoyama, H., 2021. Oxidative stress as a common key event in developmental neurotoxicity. *Jul 19 Oxid. Med Cell Longev.* 2021, 6685204. <https://doi.org/10.1155/2021/6685204>.
- Noctor, S.C., Martínez-Cerdeño, V., Ivic, L., Kriegstein, A.R., 2004. Cortical neurons arise in symmetric and asymmetric division zones and migrate through specific phases (Feb). *Nat. Neurosci.* 7 (2), 136–144. <https://doi.org/10.1038/nn1172>.
- Noor, N.A., Mohammed, H.S., Ahmed, N.A., Radwan, N.M., 2011. Variations in amino acid neurotransmitters in some brain areas of adult and young Male albino rats due to exposure to mobile phone radiation. *Eur. Rev. Med Pharm. Sci.* 15 (7), 729–742 (Jul).
- Oh, H., Lewis, D.A., Sibille, E., 2016. The role of BDNF in Age-Dependent changes of excitatory and inhibitory synaptic markers in the human prefrontal cortex (Dec). *Neuropsychopharmacology* 41 (13), 3080–3091. <https://doi.org/10.1038/npp.2016.126>. Epub 2016 Jul 15.
- Okano, H., Takashima, K., Takahashi, Y., Ojio, R., Tang, Q., Ozawa, S., Zou, X., Koyanagi, M., Maronpot, R.R., Yoshida, T., Shibutani, M., 2023. Progressive disruption of neurodevelopment by mid-gestation exposure to lipopolysaccharides and the ameliorating effect of continuous alpha-glycosyl isoquercitrin treatment (Jan). *Environ. Toxicol.* 38 (1), 49–69. <https://doi.org/10.1002/tox.23661>.
- Ortega, F., Berninger, B., Costa, M.R., 2013. Primary culture and live imaging of adult neural stem cells and their progeny. *Methods Mol. Biol.* 1052, 1–11. https://doi.org/10.1007/978-1-4939-2261-2_22. PMID: 23640252.
- Palkovits, M., 1973. Isolated removal of hypothalamic or other brain nuclei of the rat. *Sept 14 Brain Res* 59, 449–450. [https://doi.org/10.1016/0006-8993\(73\)90290-4](https://doi.org/10.1016/0006-8993(73)90290-4).
- Peerboom, C., Wierenga, C.J., 2021. The postnatal GABA shift: a developmental perspective (May). *Neurosci. Biobehav. Rev.* 124, 179–192. <https://doi.org/10.1016/j.neubiorev.2021.01.024>.
- Prochnow, N., Gebing, T., Ladage, K., Krause-Finkeldey, D., El Ouardi, A., Bitz, A., Streckert, J., Hansen, V., Dermietzel, R., 2011. Electromagnetic field effect or simply stress? Effects of UMTS exposure on hippocampal long-term plasticity in the context of procedure related hormone release. *PLoS ONE* 6, e19437. <https://doi.org/10.1371/journal.pone.0019437>.
- Ravindran, E., Arashiki, N., Becker, L.L., Takizawa, K., Lévy, J., Rambaud, T., Makridis, K.L., Goshima, Y., Li, N., Vreeburg, M., Demeer, B., Dickmanns, A., Stegmann, A.P.A., Hu, H., Nakamura, F., Kaindl, A.M., 2022. Monoallelic CRMP1 gene variants cause neurodevelopmental disorder. *Dec 13 Elife* 11, e80793. <https://doi.org/10.7554/eLife.80793>.
- Rice, D., Barone Jr., S., 2000. Critical periods of vulnerability for the developing nervous system: evidence from humans and animal models. *Jun;108 Environ. Health Perspect.* 3 (3), 511–533. <https://doi.org/10.1289/ehp.00108s3511>.
- Rowitch, D.H., Kriegstein, A.R., 2010. Developmental genetics of vertebrate glial-cell specification. *Nov 11 Nature* 468 (7321), 214–222. <https://doi.org/10.1038/nature09611>. PMID: 21068830.
- Ruediger, H.W., 2009. Genotoxic effects of radiofrequency electromagnetic fields (Aug). *Pathophysiology* 16 (2–3), 89–102. <https://doi.org/10.1016/j.pathophys.2008.11.004>.
- Rui, G., Liu, L.Y., Guo, L., Xue, Y.Z., Lai, P.P., Gao, P., Xing, J.L., Li, J., Ding, G.R., 2022. Effects of 5.8 GHz microwave on hippocampal synaptic plasticity of rats (Oct). *Int J. Environ. Health Res* 32 (10), 2247–2259. <https://doi.org/10.1080/09603123.2021.1952165>. Epub 2021 Jul 22.
- Şahin, A., Aslan, A., Baş, O., İkinci, A., Özyılmaz, C., Fikret Sönmez, O., Çolakoglu, S., Odacı, E., 2015. Deleterious impacts of a 900-MHz electromagnetic field on hippocampal pyramidal neurons of 8-week-old sprague dawley Male rats. *Oct 22 Brain Res* 1624, 232–238. <https://doi.org/10.1016/j.brainres.2015.07.042>.

- Schmahli, W., 1983. Developmental gradient of cell cycle in the telencephalic roof of the fetal NMRI-mouse. *Anat. Embryol. (Berl.)* 167 (3), 355–364. <https://doi.org/10.1007/BF00315673>.
- Schuermann, D., Mevissen, M., 2021. Manmade electromagnetic fields and oxidative Stress-Biological effects and consequences for health. *Apr 6 Int J. Mol. Sci.* 22 (7), 3772. <https://doi.org/10.3390/ijms22073772>.
- Semple, B.D., Blomgren, K., Gimlin, K., Ferriero, D.M., Noble-Haesslein, L.J., 2013. Brain development in rodents and humans: identifying benchmarks of maturation and vulnerability to injury across species (Jul-Aug). *Prog. Neurobiol.* 106–107, 1–16. <https://doi.org/10.1016/j.pneurobio.2013.04.001>.
- Sharma, A., Shrivastava, S., Shukla, S., 2021. Oxidative damage in the liver and brain of the rats exposed to frequency-dependent radiofrequency electromagnetic exposure: biochemical and histopathological evidence (May). *Free Radic. Res* 55 (5), 535–546. <https://doi.org/10.1080/10715762.2021.1966001>.
- Singh, K.V., Prakash, C., Nirala, J.P., Nanda, R.K., Rajamani, P., 2023. Acute radiofrequency electromagnetic radiation exposure impairs neurogenesis and causes neuronal DNA damage in the young rat brain (Jan). *Neurotoxicology* 94, 46–58. <https://doi.org/10.1016/j.neuro.2022.11.001>.
- Smolkin, T., Nir-Zvi, I., Duvshani, N., Mumbat, Y., Kessler, O., Neufeld, G., 2018. Complexes of plexin-A4 and plexin-D1 convey semaphorin-3C signals to induce cytoskeletal collapse in the absence of neuropilins. *May 4 J. Cell Sci.* 131 (9), jcs208298. <https://doi.org/10.1242/jcs.208298>.
- Sohal, V.S., Rubenstein, J.L.R., 2019. Excitation-inhibition balance as a framework for investigating mechanisms in neuropsychiatric disorders (Sep). *Mol. Psychiatry* 24 (9), 1248–1257. <https://doi.org/10.1038/s41380-019-0426-0>. Epub 2019 May 14.
- Sonmez, O.F., Odaci, E., Bas, O., Kaplan, S., 2010. Purkinje cell number decreases in the adult female rat cerebellum following exposure to 900MHz electromagnetic field. *Brain Res.* 1356, 95–101. <https://doi.org/10.1016/j.brainres.2010.07.103>.
- Su, L., Yimaer, A., Xu, Z., Chen, G., 2018. Effects of 1800 MHz RF-EMF exposure on DNA damage and cellular functions in primary cultured neurogenic cells (Mar). *Int J. Radiat. Biol.* 94 (3), 295–305. <https://doi.org/10.1080/09553002.2018.1432913>.
- Suto, F., Tsuboi, M., Kamiya, H., Mizuno, H., Kiyama, Y., Komai, S., Shimizu, M., Sanbo, M., Yagi, T., Hiromi, Y., Chédotal, A., Mitchell, K.J., Manabe, T., Fujisawa, H., 2007. Interactions between plexin-A2, plexin-A4, and semaphorin 6A control lamina-restricted projection of hippocampal mossy fibers. *Feb 15 Neuron* 53 (4), 535–547. <https://doi.org/10.1016/j.neuron.2007.01.028>.
- Takahashi, T., Nowakowski, R.S., Caviness Jr., V.S., 1995. The cell cycle of the pseudostratified ventricular epithelium of the embryonic murine cerebral wall (Sep). *J. Neurosci.* 15 (9), 6046–6057. <https://doi.org/10.1523/JNEUROSCI.15-09-06046.1995>.
- Tang, T., Jiao, J., Li, D., Sun, G., Lin, L., Wang, C., Wang, S., Zou, R., Liu, W., Zhao, Y., Wang, X., 2021. The function of BAP18 on modulation of androgen receptor action in luteinized granulosa cells from normal weight women with and without PCOS. *May 1 Mol. Cell Endocrinol.* 527, 111228. <https://doi.org/10.1016/j.mce.2021.111228>.
- Taschetto Vey, L., Zuquetto Rosa, H., Cristine Silva Barcelos, R., Tironi Dias, V., Izabel Ugalde Marques da Rocha, M., Escobar Burger, M., 2020. Neonatal handling increases neurogenesis, BDNF and GR in the hippocampus favoring memory acquisition in rats. *Oct 15 Brain Res* 1745, 146921. <https://doi.org/10.1016/j.brainres.2020.146921>. Epub 2020 Jun 4. PMID: 32505752.
- Tattersall, J.E., Scott, I.R., Wood, S.J., Nettell, J.J., Bevir, M.K., Wang, Z., Somasiri, N.P., Chen, X., 2001. Effects of low intensity radiofrequency electromagnetic fields on electrical activity in rat hippocampal slices. *Jun 15 Brain Res* 904 (1), 43–53. [https://doi.org/10.1016/s0006-8993\(01\)02434-9](https://doi.org/10.1016/s0006-8993(01)02434-9).
- Uchida, Y., Ohshima, T., Sasaki, Y., Suzuki, H., Yanai, S., Yamashita, N., Nakamura, F., Takei, K., Ihara, Y., Mikoshiba, K., Kolattukudy, P., Honnorat, J., Goshima, Y., 2005. Semaphorin3A signalling is mediated via sequential Cdk5 and GSK3beta phosphorylation of CRMP2: implication of common phosphorylating mechanism underlying axon guidance and alzheimer's disease (Feb). *Genes Cells* 10 (2), 165–179. <https://doi.org/10.1111/j.1365-2443.2005.00827.x>.
- Urbán, N., Guillemot, F., 2014. Neurogenesis in the embryonic and adult brain: same regulators, different roles. *Front Cell Neurosci.* 8, 396. <https://doi.org/10.3389/fncel.2014.00396>. Erratum in: *Front Cell Neurosci.* 2015 Apr 23;9:160. doi: 10.3389/fncel.2015.00160.
- Ustunova, S., Kilic, A., Bulut, H., Gurel-Gurevin, E., Eris, A.H., Meral, I., 2022. Impaired memory by hippocampal oxidative stress in rats exposed to 900 MHz electromagnetic fields is ameliorated by thymoquinone. *Toxicol. Environ. Chem.* <https://doi.org/10.1080/02772248.2022.2051509>.
- Vagnozzi, A.N., Praticò, D., 2019. Endosomal sorting and trafficking, the retromer complex and neurodegeneration (Jun). *Mol. Psychiatry* 24 (6), 857–868. <https://doi.org/10.1038/s41380-018-0221-3>.
- Valič, B., Kos, B., Gajšek, P., 2012. Occupational exposure assessment on an FM mast: electric field and Sar values. *Int J. Occup. Saf. Erg.* 18 (2), 149–159. <https://doi.org/10.1080/10803548.2012.11076924>.
- Valič, B., Kos, B., Gajšek, P., 2017. Radiofrequency exposures of workers on Low-Power FM radio transmitters. *May 1 Ann. Work Expo. Health* 61 (4), 457–467. <https://doi.org/10.1093/annweh/wxx012>.
- Verschaeve, L., Juutilainen, J., Lagroye, I., Miyakoshi, J., Saunders, R., de Seze, R., Tenforde, T., van Rongen, E., Veyret, B., Xu, Z., 2010. *in vitro* and *in vivo* genotoxicity of radiofrequency fields. *Mutat. Res./Rev. Mutat. Res.* 705, 252–268. <https://doi.org/10.1016/j.mrrev.2010.10.001>.
- Wang, H., Liu, Y., Sun, Y., Dong, J., Xu, X., Wang, H., Zhao, X., Zhang, J., Yao, B., Zhao, L., Liu, S., Peng, R., 2023. Changes in cognitive function, synaptic structure and protein expression after long-term exposure to 2.856 and 9.375 GHz microwaves (Feb). *Cell Commun. Signal* 21 (1), 34. <https://doi.org/10.1186/s12964-022-01011-1>.
- Wang, Y., Wang, C., Ranefall, P., Broussard, G.J., Wang, Y., Shi, G., Lyu, B., Wu, C.T., Wang, Y., Tian, L., Yu, G., 2020. SynQuant: an automatic tool to quantify synapses from microscopy images. *Mar 1 Bioinformatics* 36 (5), 1599–1606. <https://doi.org/10.1093/bioinformatics/btz760>.
- Wong, T.P., Marchese, G., Casu, M.A., Ribeiro-da-Silva, A., Cuello, A.C., De Koninck, Y., 2006. Imbalance towards inhibition as a substrate of aging-associated cognitive impairment. *Apr 10-17 Neurosci. Lett.* 397 (1-2), 64–68. <https://doi.org/10.1016/j.neulet.2005.11.055>.
- Wu, H., Min, D., Sun, B., Ma, Y., Chen, H., Wu, J., Ren, P., Wu, J., Cao, Y., Zhao, B., Wang, P., 2023. Effect of WiFi signal exposure in utero and early life on neurodevelopment and behaviors of rats (Sep). *Environ. Sci. Pollut. Res Int* 30 (42), 95892–95900. <https://doi.org/10.1007/s11356-023-29159-4>.
- Xu, F., Bai, Q., Zhou, K., Ma, L., Duan, J., Zhuang, F., Xie, C., Li, W., Zou, P., Zhu, C., 2017. Age-dependent acute interference with stem and progenitor cell proliferation in the hippocampus after exposure to 1800 MHz electromagnetic radiation. *Electro Biol. Med* 36 (2), 158–166. <https://doi.org/10.1080/15368378.2016.1233886>.
- Yamashita, N., Goshima, Y., 2012. Collapsin response mediator proteins regulate neuronal development and plasticity by switching their phosphorylation status (Apr). *Mol. Neurobiol.* 45 (2), 234–246. <https://doi.org/10.1007/s12035-012-8242-4>.
- Zahr, S.K., Kaplan, D.R., Miller, F.D., 2019. Translating neural stem cells to neurons in the mammalian brain (Dec). *Cell Death Differ.* 26 (12), 2495–2512. <https://doi.org/10.1038/s41418-019-0411-9>. Epub 2019 Sep 24. PMID: 31551564; PMCID: PMC7224185.
- Zeiss, C.J., 2021. Comparative milestones in rodent and human postnatal central nervous system development (Dec). *Toxicol. Pathol.* 49 (8), 1368–1373. <https://doi.org/10.1177/01926233211046933>.
- Zhang, W., Liu, H., 2002. MAPK signal pathways in the regulation of cell proliferation in mammalian cells. *Cell Res* 12, 9–18. <https://doi.org/10.1038/sj.cr.7290105>.
- Zhang, Y.L., Deng, L., Liao, L., Yang, S.Y., Hu, S.Y., Ning, Y., Zhang, F.L., Li, D.Q., 2022. Chromatin complexes subunit BAP18 promotes triple-negative breast cancer progression through transcriptional activation of oncogene S100A9. *Apr 28 Cell Death Dis.* 13 (4), 408. <https://doi.org/10.1038/s41419-022-04785-x>. PMID: 35484101; PMCID: PMC9050672.
- Zheng, R., Zhang, X., Gao, Y., Gao, D., Gong, W., Zhang, C., Dong, G., Li, Z., 2023. Biological effects of exposure to 2650 MHz electromagnetic radiation on the behavior, learning, and memory of mice (Jun). *Brain Behav.* 13 (6), e3004. <https://doi.org/10.1002/brb3.3004>.